# MUSCLE MODELLING, ANALYSIS AND SIMULATION OF A PHYSIOLOGICAL MOTOR CONTROL SYSTEM

**ARMEEN SAEED**

**01-244221-001**


**Department of Electrical Engineering,**

**Bahria University, Islamabad**

**2024**

# MUSCLE MODELLING, ANALYSIS AND SIMULATION OF A PHYSIOLOGICAL MOTOR CONTROL SYSTEM

**ARMEEN SAEED**

**01-244221-001**

**Supervised by: Dr. Nadia Imran**

**Co-Supervised by: Dr. Muhammad Najam-ul-Islam**

A thesis submitted in fulfillment of requirements for the award of the degree of

Masters of Science (Electrical Engineering)

**Department of Electrical Engineering,**

**Bahria University, Islamabad**

**2024**

# THESIS COMPLETION CERTIFICATE

**Student's Name:** Armeen Saeed

**Registration No:** 01-244221-001

**Program of Study:** MS Electrical Engineering

**Thesis Title:** MUSCLE MODELLING, ANALYSIS AND SIMULATION OF A PHYSIOLOGICAL MOTOR CONTROL SYSTEM

It is to certify that the above scholar's thesis has been completed to my satisfaction and, to my belief, its standard is appropriate for submission for Evaluation. I have also conducted plagiarism test of this thesis using HEC prescribed software and found similarity index at 13% that is within the permissible limit set by the HEC for the MS/MPhil degree thesis. I have also found the thesis in a format recognized by the BU for the MS/MPhil thesis.

Supervisor's Signature: _____

Name: Dr. Nadia Imran

Date: _____

# AUTHOR'S DECLARATION

I, <u>Armeen Saeed</u>, hereby certify that all material in this dissertation titled "<u>MUSCLE MODELLING, ANALYSIS AND SIMULATIONS OF A PHYSIOLOGICAL MOTOR CONTROL SYSTEM</u>" is my own work and has not been submitted previously by me for taking any degree from <u>Bahria University, Islamabad</u> or elsewhere in the country/world.

At any time, if my statement is found to be incorrect the university has the right to withdraw/cancel my MS degree.

Scholar's Signature: _____

Name of Student: <u>ARMEEN SAEED</u>

Date: _____

# PLAGIARISM UNDERTAKING

I, solemnly declare that research work presented in the thesis titled "<u>MUSCLE MODELLING, ANALYSIS AND SIMULATIONS OF A PHYSIOLOGICAL MOTOR CONTROL SYSTEM</u>" is solely my research work with no significant contribution from any other person. Small contribution / help wherever taken has been duly acknowledged and that complete thesis has been written by me.

I understand the zero-tolerance policy of the HEC and Bahria University towards plagiarism. Therefore, I as an Author of the above titled thesis declare that no portion of my thesis has been plagiarized and any material used as reference is properly referred / cited.

I undertake that if I am found guilty of any formal plagiarism in the above titled thesis even after award of PhD degree, the university reserves the right to withdraw / revoke my PhD degree and that HEC and the University has the right to publish my name on the HEC / University website on which names of scholars are placed who submitted plagiarized thesis.

Scholar / Author's Sign: _____

Name of the Scholar: <u>ARMEEN SAEED</u>

# LIST OF PUBLICATIONS

I would like to acknowledge that the work in this thesis has been submitted for publication to the Biological Cybernetics entitled as "Bond Graph Analysis of a Three-Link Physiological Motor Control System: Integrating Simulation and Muscle Behavior" and is under peer review.

# DEDICATION

I dedicate this thesis to my beloved parents who have offered unconditional love and support and have always been there for me.

# ACKNOWLEDGEMENT

I am very grateful to Almighty Allah, who is the most merciful and beneficent, who has blessed me with all His blessings and helped me and gave me strength to carry out this dissertation work.

I would like to thank my beloved family members without their constant support and cooperation I would not be able to achieve so much in life.

I want to express my gratitude to my supervisor, Dr. Nadia Imran, and co-supervisor, Dr. Najam-ul-Islam, for supervising and mentoring me during the entire process, for their patience, motivation and immense knowledge, enabling me to complete this work.

Lastly, I would like to acknowledge the contributions of Dr. Asif Mahmood Mughal. His expertise, constructive feedback, and dedication significantly enriched the quality of this work.

I am truly fortunate to have had Dr. Nadia Imran as my mentor, and I extend my deepest appreciation for her contributions to the successful completion of this thesis.

# ABSTRACT

Understanding the process of standing up from a sitting position involves complex biomechanical interactions. Traditional models in biomechanics, which focus on basic movements, often fail to capture the intricate role of muscles. This study improves on current models by concentrating on the contribution of muscles to sit-to-stand movement, specifically addressing three joints in the sagittal plane (hip, knee, and ankle). Bond graph modelling (BGM) and Hill-type muscle models are used in the study to generate a more realistic representation of the sit-to-stand action. This work emphasizes on the alternate Hill-type model that helps to achieve a more thorough knowledge of muscle mechanics. The complete bond graph model is divided into two subsystems combined with PID-controllers, one is the actual system which represents the physiological framework and second is the virtual system which mimics the behavior of Central Nervous System (CNS). It is observed that lower torque results are achieved by the inclusion of muscles in the system as compared to earlier studies. This advancement directs the way toward a more individualized and successful rehabilitation processes, with important applications targeting rehabilitation robotics. The research adds to the creation of better assistive devices and rehabilitation programs by giving a more realistic model of human mobility. In conclusion, this work introduces an improved method to biomechanical modelling that provides a better understanding of the sit-to-stand action. It questions existing models and suggests a more thorough technique, bringing up new options for biomechanics and rehabilitation research.

# TABLE OF CONTENTS

# LIST OF TABLES

# LIST OF FIGURES

# LIST OF SYMBOLS

| | | |
|---|---|---|
| R | - | Damping element |
| C | - | Compliance element |
| Se | - | Source of effort |
| Sf | - | Source of flow |
| MSe | - | Modulated source of effort |
| I | - | Inertial element |
| $x$ | - | Translational momentum |
| $\theta$ | - | Angle |
| $\omega$ | - | Angular velocity |
| $\bar{r}$ | - | Relative position |
| $\tau$ | - | Torque |
| T | - | Force |
| $\bar{q}$ | - | Rotational momentum |
| TF | - | Transformer |
| MTF | - | Modulated transformer |

# CHAPTER 1

# INTRODUCTION

Exploring the complexities of human movement and its accurate representation in biomechanical models is a challenge that has captivated researchers for decades. In this work, we delve into one of the most fundamental and intricate movements – the sit-to-stand motion – and seek to enhance its modelling through the integration of muscle dynamics. The aim of this work not only fills current gaps in biomechanical modelling, but it also lays the path for breakthroughs in disciplines such as rehabilitation robots and human motion analysis.

## 1.1 Background

The way humans move from sitting to standing has always interested the study of human movement. This is very important in a field called biomechanics that looks at how our bodies work. This simple move needs help from many parts of the body like muscles, joints and brain connections. This is not just needed for daily life but also in healing processes.

In the past, stiff body models have been very helpful to understand how human bodies move. These studies have limits when looking into the details of how muscles contribute to moves. Some studies look at the role of muscles but generally are only focused on single joint analysis.

## 1.2 Research gap

This study presents a novel approach aimed at tackling the lack of muscle involvement. It does this by using bond graph modelling (BGM) to model these complex connections between muscles. This study focuses on adding muscle actions to body

movement models, paying special attention to joint angles and forces when you get up from sitting.

The novelty about this method is that it lets us see how people really move in life and gives a more near to precise results. It goes beyond old ways of showing things, which often make them too simple. The previous studies generally focus on the study of single joint muscle contribution and this study aims to target major three joints (Hip, Knee and ankle) involved in sit-to-stand motion.

## 1.3 Proposed methodology

This study's approach is novel, using BGM and Hill-type muscle models. BGM, which is flexible in system dynamics, offers a way to show how a system's many energy exchanges and connections occur. It gives a detailed look at how parts of the body's muscle and bone system work together when you move, if we talk about biomechanics.

Using Hill-type muscle models improves how real the simulations seem. These models, which are like real muscles, help us to know how muscle strength changes with length and speed. This is important for understanding human movements in action.

Main focus of this study will be to target three joints of the lower body during sit-to-stand motion and try to achieve better torque values in simulations resulting in decoding a more near to human like motion.

## 1.4 Model implementation and assessment

To calculate the precise torque required for sit-to-stand movement, the model will be evaluated at the hip, knee, and ankle joints. The model's sensitivity to changes in crucial elements such as muscle activation and joint angles will be tested. In addition, the effect of varying joint angles on the system's needed torque will be examined.

This study used a three-link biomechanical model consisting of foot, leg, thigh, and head-arm-trunk (HAT) in the sagittal plane to apply the aforementioned model. Figure 1 depicts the segmentation of the human body, with one segment defined as head-arm-trunk, another as hip-knee, another as knee-ankle, and the final as foot.

## 1.5 Employing the alternate Hill-type muscle model

The Hill-type model is a popular way to depict how muscles actually work. It is known for its ability to pretend that muscle force changes with length and speed of action. This other study, however, uses a new way. It applies the different Hill-type muscle model. This new way of thinking explains muscle work better. It's great for studying movements like standing up from a sitting position. It helps us better understand how muscles make force and control movement, which is very important for real and accurate models.

Adding the different Hill-type muscle model to BGM is a big move forward. BGM, famous for showing energy changes in hard systems, is great for looking at the complex movements of muscle and joint and brain connections in people. This combination gives a complete tool for looking at how muscles help with joint forces and angles. This is important in understanding the mechanics of sitting down and standing up movements.
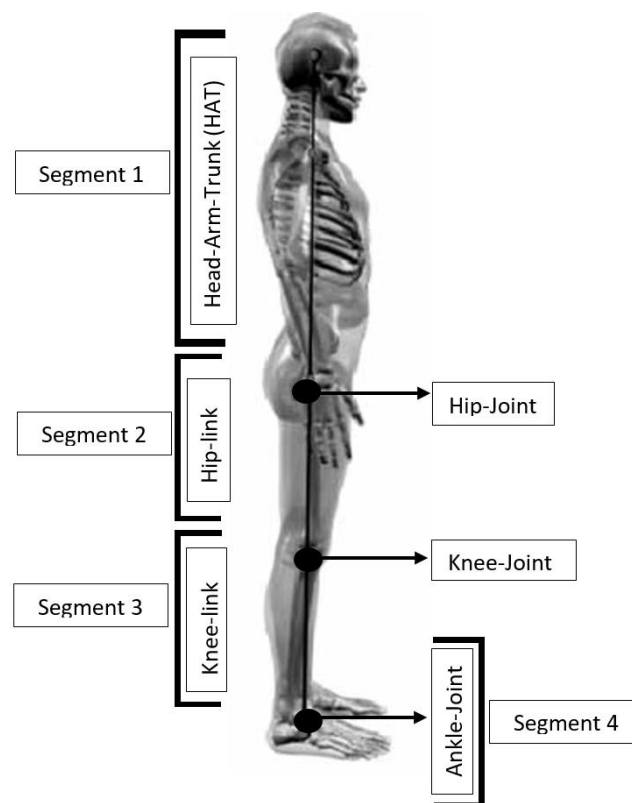


**Figure 1** Segmentation of the body

## 1.6 Impact on rehabilitation robotics

In robotics for rehabilitation, this advanced understanding is very important. Often, current technology has problems because old designs don't understand how muscles work and change. This study makes it possible to build better rehabilitation devices and strategies. It does this by giving a more clear and full model. This study lays the way for the creation of more effective rehabilitation equipment and approaches that are customized to individual requirements and situations by giving a more precise and thorough model.

It is very important in rehabilitation robotics to focus on adding joint movements and forces of muscles. These guidelines are necessary for creating help tools and recovery plans. Knowing more about how joints work can help create better recovery treatments that fit each person's unique needs. This is very helpful for people who are healing from injuries or have trouble moving around.

## 1.7 Contribution to the field and future directions

This research contributes to the academic content of biomechanics as well as its practical uses. It challenges present models and ideas about human mobility and suggests a fuller method. This work not only describes an innovative model but also provides a comprehensive theoretical and practical study of its implications. It creates opportunities for future study, encouraging more research on the incorporation of muscle dynamics in biomechanical models.

In subsequent chapters, this work will delve into this new approach's technique, simulations, outcomes, and implications. It will discuss the technical aspects of BGM and Hill-type muscle models, as well as a method for determining joint angles and torques computed, along with the significance of these findings in terms of biomechanics and rehabilitation. Such research is not only an academic pursuit but a way to the future where rehabilitation got more efficient, customized and based on a fundamental comprehension of human movement.

# CHAPTER 2

# LITERATURE REVIEW

This section discusses the review of the literature studies existing evidence in control systems and biomechanics, with particular focus on refinements that cast light upon and broaden the field of rehabilitation robots.

## 2.1 Bond graph modelling in biomechanics

BGM has a novel application in biomechanical study. It is an approach that has redefined how interrelated mechanical and electrical systems are regarded given human movement where Soni and Vaz (2021) marked a turning point.

They have conducted groundbreaking research in measuring knee joint torques during Sit-to-Stand and Stand-to-Sit motions, establishing a standard within this industry. They found not only the mechanisms but an entire system, which allows for detailed injection of muscle dynamics into biomechanical models.

## 2.2 Delving into muscular dynamics

Biomechanical modelling depends on deep knowing of muscle activity. 1989 was the year of Zajac's seminal work in which he proposed Hill's alternative muscle model. And it's not just a model; it can be seen as a lens through which muscle action can be observed in unprecedented detail. It focuses on the intricate operations of muscles and their essential role in biomechanical mimicking. Zajac (1989) sets the ground for this study, making a thorough implementation of Hill's model in bond graph framework and uncovers the intricate patterns there exists between muscles and joints during normal motions.

## 2.3 Recent advancements in human motion simulation

BGM has come a long way in the last decade, particularly on mirroring muscle-driven joint movements. The work done by Smith et. al. (2021) pushes the boundaries further with approaches that shed light on the small but crucial role of muscles in joint torque measurement. Continuing with the creative mindset, this work develops Soni and Vaz (2021) model by integrating anatomically accurate muscle models to better depict torque dynamics during human movement.

## 2.4 Joint torque – An approach integrating multiple disciplines

Johnson et al. in 2021 correctly captured the multidimensional nature of joint torque estimation. Their in-depth study incorporates an array of approaches, from musculoskeletal models to advanced machine learning methods. Such a study as this, integrates muscle models within the bond graph framework to offer more advanced approach on how joint torque can be estimated.

## 2.5 Bridging theory and experimentation

A groundbreaking study by Chen et al. 2020 shows the strength of marrying computational models with experimental data. This synergy is crucial to enhance the precision of biomechanical simulations. Inspired by their approach, this research aims at combining theoretical modelling with real-world data thus improving the bond graph models by including detailed muscle dynamics so as to facilitate better understanding of knee joint torque while in motion.

## 2.6 Uncharted territories in joint torque dynamics

A review of the previous researches reveals critical gaps, in particular, deep analysis of muscle torque interactions and use of muscle dynamics to calculate joint torques. F. Kitayama, R. Kondo, and R. Endo's work in 2023 focus on enhancing transmission torque characteristics in strain wave gears using magnets, as they provide new dimensions to torque dynamics and the possibility for further investigation into joint torque changes from a magnetic enhancement perspective.

Similarly, Wakeling et al.'s 2023 review and Sultan et al.'s 2021 study illustrate the changing landscape of muscle and musculoskeletal models, emphasizing the necessity for more detailed research into muscle behavior's direct influence on joint torque.

## 2.3 Earlier studies: insights, methodologies, contributions, and research gaps

Several key research in the realm of controls have made substantial contributions to understanding torque dynamics and associated approaches. The following research works demonstrate diverse views and gaps that have prompted the need for more study.

Kitayama et al. (2023) present a novel method for increasing transmission torque in strain wave gears by employing magnets. It is a huge step forward in gear technology. However, its application to human joint biomechanics remains unexplored, notably in estimating detailed joint torques. This approach is used in our study, and it is extended to understand how such improvements in torque transmission might be replicated in human joint dynamics, which is an important component in biomechanical simulations.

Wakeling and colleagues (2023) paper provides a detailed historical review of muscle and musculoskeletal models. Their research, while broad, falls short of investigating the direct link between individual muscles and joint torque dynamics. Our study will go into these precise correlations, concentrating on the intricacies of muscle dynamics in the sit-to-stand action, thereby addressing a critical gap they found.

Smith et al. (2022) make a significant contribution by developing BGM for mimicking muscle-driven joint motions. While they made major advances in including specific muscle dynamics, our study goes a step further by tackling the obstacles in capturing the whole spectrum of muscle action and its influence on joint torque, resulting in a more comprehensive understanding.

Sultan et al. (2021) emphasized the complexities of neuromuscular connections by investigating nonlinear postural control with neural delays. Our research expands on this by investigating how neural delays affect muscle contributions to joint torques under substantial perturbations, therefore improving our knowledge of neuromuscular control in biomechanics.

Johnson et al.'s (2021) interdisciplinary work synthesizes multiple approaches for joint torque estimation. However, it does not fully account for the role of muscle

dynamics. Our study fills this gap by focusing on muscle dynamics in prediction of joint torque that will advance the field toward more realistic biomechanical models.

The reference model employed in our research is the bond graph model for Sit-to-Stand (SiTSt) and Stand-to-Sit (StTSi) movements developed by Soni and Vaz (2021). Improve their work by incorporating individual muscle contributions in joint torque calculations leading to better utility of the model during biomechanical investigations.

Rafique S. et al (2020) conducted research on neuro-fuzzy control of sit-to stand motion using head position tracking. The present study will develop a modeling framework to assess the contribution of head position trajectory during sit-to stand (STS) movement governed by the central nervous system. Based on the research, slow dynamics of CNS also contribute to generating suitable joint angles for necessary head position during STS. The authors validate their modeling scheme with a biomechanical model and adaptive neuro-fuzzy inference system controllers.

The contributions of Chen et al. 2020 and Tan 2020 are significant in biomechanics, with the former working on combining computer models with empirical data and the latter who builds an exoskeleton for rehabilitation. Our study contributes to the gap in previous research by thoroughly exploring the intricacies of muscle behavior in calculating joint torque, insights which are critical for successful rehabilitation methods.

Useful insights on BGM are provided by Mughal and Iqbal 2006 as well as Zoheb and Mughal 2013. These works demonstrate the possible applications of BGM in biomechanical systems. However, they do not fully delve into the role of muscles in joint torque calculation. Our study meets this demand by ensuring a good understanding of muscle dynamics in biomechanical models.

This detailed review of available literature identifies the progress and constraints in establishing our comprehension of muscle dynamics evolution and joint torque estimations in biomechanics. The studies reviewed provide a background for our study as they address the key areas that have remained elusive thus far. Methods. The next section will examine the methods used as we move from the theoretical foundations provided by these books to practical application in our analysis. This will include our new approach in integrating muscle dynamics into BGM as a path towards enhancing the performance and usability of biomechanical models across theoretical and practical domains.

# CHAPTER 3

# METHODOLOGY

This research builds on the bond graph model proposed by Soni and Vaz 2021 for sit-to-stand and stand-to-sit movement, seeking to integrate specific muscle dynamics at any given joint. We describe the specifics of the integration process into 20-sim platform, focusing on muscle dynamics complexities and their influence on joint torque during Sit-to-stand motions.

## 3.1 System segmentation and subsystems for the Sit-to-Stand dynamics

The system for modelling the dynamics of Sit-to-stand motions comprises two identical subsystems. These are named the virtual subsystem and the actual subsystem. The virtual subsystem imitates the working of the Central nervous system (CNS). It represents an imaginary human body. The actual subsystem represents the real human body.

The virtual subsystem is nominally similar to the actual subsystem in terms of mass and inertial properties. The subsystem comprises of one rigid link and three muscular links representing the upper body i.e. HAT (head, arms and trunk), hip, knee and ankle respectively, connected by revolute joints. For illustration purposes figure 1 represents the segmentation of our model in the sagittal plane.
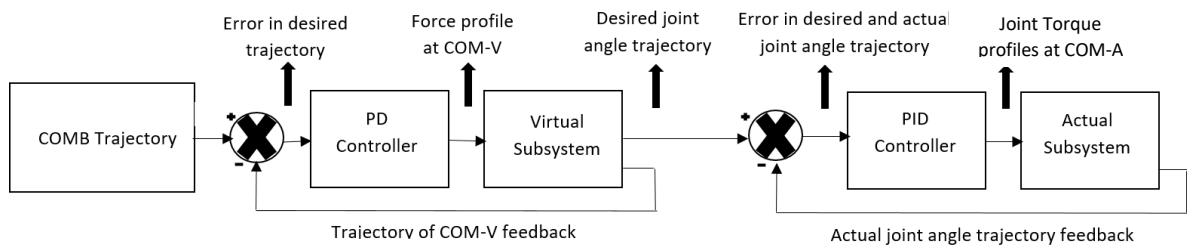


**Figure 2** Schematic of model. Each subsystem of the model is represented in the blocks,

The complete bond graph model for Sit-to-stand motions comprises two sub-models: one is a model of the virtual subsystem (model-V) and the other is a model of the actual subsystem (model-A). To emulate the working of the CNS, the centre of mass of the model-V (COM-V), is moved through a PD controller along the experimentally determined trajectory of the COMB as shown in figure 2. For comparison purposes, results are taken from Soni & Vaz (2021).

These joint angle trajectories are commanded to the PID controllers at each joint which act as actuators and mimic the function of muscles. Consequently, PID controllers provide the required joint torques at each joint such that the Centre of mass of the actual subsystem (COM-A) tracks the trajectory of COM-V. Thus, COM-A follows the desired trajectory of COMB.

All processes; from the imposition of desired trajectory on the COM-V, calculation of respective joint angles, commanding those joint angles to the PID controllers and application of torques by PID controllers on respective joints of model-A are simultaneous. All the subsystems shown in figure 2 are explained in detail in the subsequent sections of this paper. The next section elaborates on the subsystems considered for the modelling.

### 3.2 Anthropometric properties of the subsystems

The Anthropometric properties of both actual and virtual subsystems have been taken according to Dumas and Wojtusch (2017). The segmental reference frames are the frames on the segments considered by Dumas and Wojtusch in their work. The arrangement of those segmental reference frames considered by Dumas and Wojtusch is different from the body frames considered in the present work. This is because, Dumas and Wojtusch fixed their segmental frames according to the International Society of Biomechanics (ISB) whereas, in the present work, body frames are fixed according to the Denavit–Hartenberg (D-H) convention.

The Denavit-Hartenberg (D-H) parameters consists of four parameters used to describe the kinematic relationship between two of rigid bodies either in a robotic manipulator or in any mechanical system. They are as follows:

1. Link length (a): The distance between two consecutive joint axes along the common normal.

2. Link twist (α): The angle between two consecutive joint axes about the common normal.

3. Link offset (d): The distance between two axes joined together along the pre-existing z-axis.

4. Joint angle (θ): The angle of rotation about the previous z-axis to align the current and previous joint axes.

By substituting these parameters, the transformation matrix of the adjacent frames is easily calculated and this also helps in the analysis of the system`s kinematics. With the use of D-H convention a complex robotic system can be reduced into a simple model and now it is an established method in robotics and biomechanical research.

The D-H convention of fixing the body frames is more advantageous for the kinematic analysis of the system, as the complete kinematics of the system can be defined using only four quantities, in terms of joint variables and link parameters. Figure 3 shows the different segments and the segmental frames considered by Dumas and Wojtusch (2017).
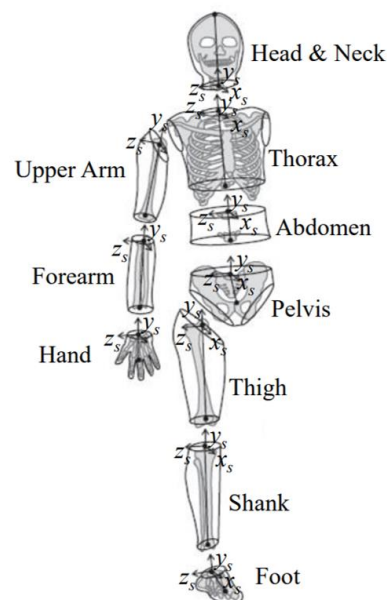


**Figure 3** Segments and segmental frames by Dumas and Wojtusch (2017)

Segment 4, of the seven-link actual subsystem, includes all the segments of the upper body given by Dumas and Wojtusch (2017) as represented in figure 3. There are a total of 8 segments of the upper body: the pelvic, abdomen, thorax, head and neck, upper arm, forearm, and hand. The position of the Centre of mass of each upper body segment with respect to its respective segmental reference frame is calculated according to Dumas and Wojtusch (2017). Bond graph model of the system discussed in detail is explained in the next chapter.

## 3.3 Integration of Hill-type muscle models

The Hill-type muscle models are integrated at key joints (hip, knee, and ankle) to simulate muscle force generation and interaction with skeletal elements. This involves modelling the muscles' force-length and force-velocity relationships, crucial for replicating realistic muscle behavior during movements. We aim to enhance the biomechanical model by incorporating realistic muscle dynamics at the key joints. This is achieved through the following steps:

- Modelling Muscle Mechanics: Each muscle is represented using the Hill-type model, which captures the force-length and force-velocity relationships. This is crucial for simulating how muscles contract and generate force during movements.

- Parameter Selection: Parameters such as maximum muscle force, optimal fiber length, and tendon slack length are carefully selected based on physiological data. These parameters are critical for accurately modelling the behavior of different muscles.

- Muscle-Joint Interaction: The interaction between muscle forces and joint movements is modeled. This includes calculating how muscle forces contribute to the torques at each joint during different phases of the sit-to-stand and stand-to-sit movements.

- Integration with the Skeletal Model: The muscle models are integrated into the existing skeletal model of the bond graph framework. This integration allows for the simulation of combined muscle and skeletal dynamics, providing a more comprehensive representation of human movement.

Hill-type muscle models with active and passive components are used to describe muscle forces as illustrated in figure 4. In these models, compliance is denoted by C, and it is represented in series elements as Cs and in parallel elements as Cp. The force acting on the muscle is generated by an external source denoted by Se.



**Figure 4** a) Block diagram of 1st Hill model. b) Block diagram of Alternate Hill model.

The methodology adopted for this study is designed to bridge the identified gaps in prior research while leveraging and integrating the strengths observed in existing methodologies. Emphasizing a comprehensive approach, this section elucidates the research design, data collection techniques, and analytical frameworks employed to delve deeper into the intricacies of muscular dynamics and their pivotal role in joint torque estimations. In the next section, we will discuss the bond graph model of each sub-model.

# CHAPTER 4

# BOND GRAPH MODELLING

A systematic approach has been followed to develop the bond graph model for the dynamics of Sit-to-stand motion. Initially, a bond graph model of a rigid link (RL) is developed (Mishra & Vaz, 2017; Pathak & Vaz, 2020) which Soni & Vaz (2021) have utilized and created a model for their research. However, the model used in Soni & Vaz (2021) does not incorporate dynamics of muscles.

Next, the novelty of this research, rigid links embedded with the alternate hill type muscle model to simulate the behavior of muscles is developed. Lastly, the model of a revolute joint constituting the bond graph model of translational coupling (TC) and bond graph model of conditional rotational coupling (CRC) is developed. Subsequently, those bond graph models are appropriately assembled together to develop the complete bond graph sub-models of the actual and virtual subsystems.

It has already been explained in chapter 3 that the complete dynamic model comprises model-V which imitates the working of the CNS, and the model-A representing the human body. Though most of the structure of model-V and model-A is similar, there are subtle differences between the two which are discussed subsequently.

Complete bond graph model-V and model-A are discussed towards the end of this section. In all bond graph models, throughout the paper, the thick bonds represent multi-bonds having a cardinality of 3, and the thin bonds are scalar bonds. All of the segments of the model are described below in detail.

## 4.1 Bond graph modelling of a rigid link

The development of the bond graph of the link can be started with the flow mapping technique based on kinematics. Only reference frame is considered rigid. Therefore, the

velocity of a point of Model-A observed and expressed in the inertial frame can be represented as:

$$^0_0\dot{r}_{HAT\_Aa} = {}^0_0\dot{r}_{HAT\_Ac} - \left[ {}_{HAT\_Ac}{}^0\bar{r}_{HAT\_Aa} \times \right] {}^0_0\dot{\omega}_{HAT\_A} \tag{1}$$

Where $^0_0r_{Ac}$ is the velocity of the center of mass of the upper body link, and $^0_0\omega_{HAT\_A}$ is its angular velocity observed and expressed in inertial reference frame. $\left[ {}_{HAT\_Ac}{}^0\bar{r}_{HAT\_Aa} \times \right]$ is a skew-symmetric matrix calculated from the position vector given as:

$$_{HAT\_Ac}{}^0\bar{r}_{HAT\_Aa} = \{ {}_{HAT\_Ac}{}^0x_{HAT\_Aa} \quad {}_{HAT\_Ac}{}^0y_{HAT\_Aa} \quad {}_{HAT\_Ac}{}^0z_{HAT\_Aa} \}^T \tag{2}$$

$$_{HAT\_Ac}{}^0\bar{r}_{HAT\_Aa} = \left[ {}_{HAT\_A}{}^0R \right] {}^{HAT\_A}_{HAT\_Ac}\bar{r}_{HAT\_Aa} \tag{3}$$

Where $_{HAT\_Ac}{}^0\bar{r}_{HAT\_Aa}$ is the position of iA point of the Model-A link with respect to its center of mass and expressed in its body frame {HAT_A}. $\left[ {}_{HAT\_A}{}^0R \right]$ is a rotation matrix representing the orientation of the {iA} body frame with respect to the inertial frame {0}. $\left[ {}_{HAT\_A}{}^0R \right]$ is calculated by integrating $\left[ {}_{HAT\_A}{}^0\dot{R} \right]$.

$$\left[ {}_{HAT\_A}{}^0\dot{R} \right] = \left[ {}_{HAT\_A}{}^0\overline{\omega_{HAT\_A}} \times \right] \left[ {}_{HAT\_A}{}^0R \right] \tag{4}$$

Similarly, the velocity of point iAb of the iA link is calculated.
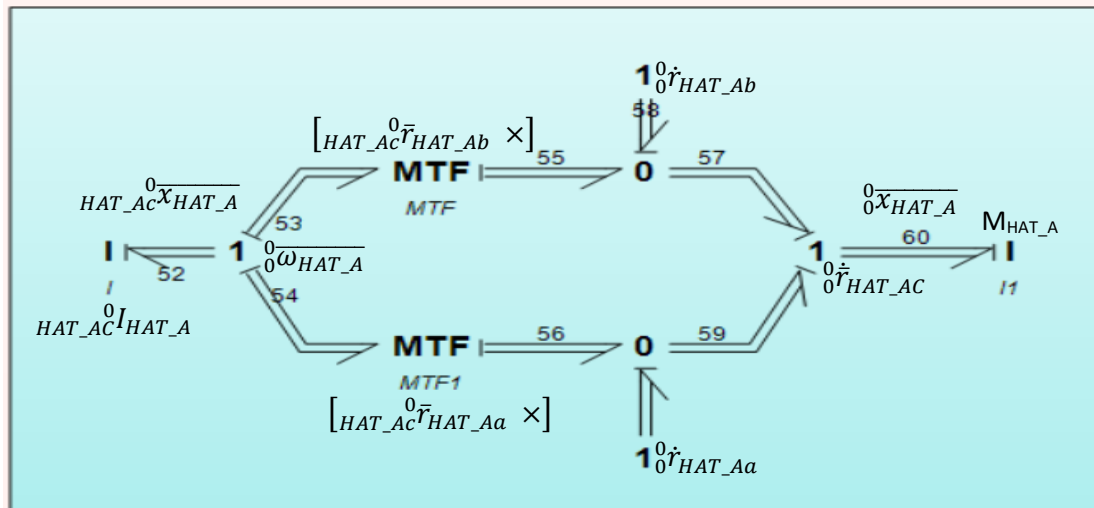


**Figure 5** Rigid link of the model, serves as the upper body frame for our research

The bond graph representation of the velocities of points HAT_Aa and HAT_Ab of the model-A link is illustrated in figure 5. $1^0_0\dot{r}_{HAT\_Aa}$ and $1^0_0\dot{r}_{HAT\_Ab}$ are common flow

junctions representing the velocity of the centre of mass of the iAth link and its angular velocity.

Further, bond graph dynamics of the rigid-link is obtained by adding inertial elements I: $M_{HAT\_A}$, I: $_{HAT\_AC}^{\quad 0}I_{HAT\_A}$ and the causal strokes. Where I: $_{HAT\_AC}^{\quad 0}I_{HAT\_A}$ represents the rotational inertial element and I: $M_{HAT\_A}$ represents the translational inertial element.

## 4.2 Bond graph modelling of muscular link

Figure 6 shows the Bond graph of muscular link. By modifying the rigid-link and incorporating muscles using alternate hill type muscle model, muscular link is obtained. Using standing position as reference ($\theta$=0 degrees) and we have to stabilize the system at standing position. The constant reference input in figure 6 is taken as zero. The reason for such reference input is that our final position is static. Input signal is fed to 2nd Hill type Muscle model.

The values of B, Cs, Cp, m, m1, m2, Rsp, Csp, Csr, Bgto and Cgto are taken from Zoheb, Madiha (2013). In this muscle model m1 is the weight of muscle and m2 is mass of human body. There is a 10% tolerance margin in the mass of the body. This tolerance is catered as disturbance in the system. This disturbance is presented in the system as modulated source of effort "constant".
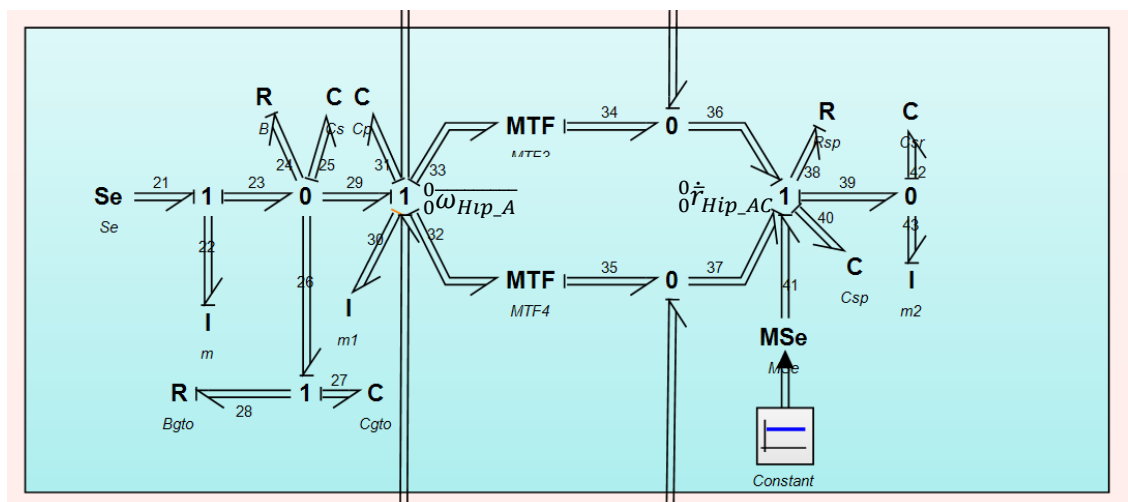


**Figure 6** Bond graph model of muscular link

GTO detects variations in muscle tension and relays this information to the brain. In our scenario, the brain will be model-V, which will be explored more at the end of the section. The GTO model is described in Zoheb (2013). This model takes flow from muscle structure as input.

As detailed by Mughal, Asif M., & Iqbal, K. (2013), the order of the system is reliant on the order of each subsystem. The muscle structure is third order, GTO is first order system, and simplified third order muscle spindle structure. The musculoskeletal system shown in figure 6 is given in (5)-(13). This is similar to that of given by Mughal, Asif M., & Iqbal, K. (2013) with a slight change that these bonds are multi bonds with a cardinality of 3 and the inclusion of $CRC_i$ and $TC_i$ elements in (9).

$$\dot{P}_{22} = Se - \frac{q_{25}}{C_s} \tag{5}$$

$$\dot{q}_{25} = \left(\frac{p_{22}}{m} - \frac{1}{B}\right) - \left[\left(\frac{q_{25}}{C_s} - \frac{q_{27}}{C_{gto}}\right) \times \left(\frac{1}{B_{gto}}\right)\right] + \frac{p_{30}}{m_1} \tag{6}$$

$$\dot{q}_{31} = \frac{p_{38}}{m_1} \tag{7}$$

$$\dot{q}_{27} = \left(\frac{q_{25}}{C_s} - \frac{q_{27}}{C_{gto}}\right) \times \frac{1}{B_{gto}} \tag{8}$$

$$\dot{P}_{30} = CRC_i - \left(\frac{q_{31}}{C_p} + CRC_{i-1}\right) - \frac{q_{27}}{C_{gto}} + TC_i \tag{9}$$

$$\dot{P}_{43} = \frac{q_{42}}{C_{sr}} \tag{10}$$

$$\dot{q}_{40} = \frac{1}{R_{sp}} \times \left(\left(Constant + \frac{q_{25}}{C_s} - \frac{q_{27}}{C_{gto}}\right) + \left(TC_i - \frac{q_{40}}{C_{sp}} - \frac{q_{42}}{C_{sr}} - \frac{q_{31}}{C_p}\right)\right) \tag{11}$$

$$\dot{q}_{42} = \frac{1}{R_{sp}} \times \left(\left(Constant + \frac{q_{25}}{C_s} - \frac{q_{27}}{C_{gto}}\right) + \left(TC_i - \frac{q_{40}}{C_{sp}} - \frac{q_{42}}{C_{sr}} - \frac{q_{31}}{C_p}\right)\right) - \frac{p_{43}}{m_2} \tag{12}$$

This model's output is a message to the brain. Translational flow and effort are the outputs of the muscle model. This muscle model is linked to the HAT, which, as previously explained, requires rotational and translational inputs. This output is sent into the HAT structure, coupled with a constant1 source of effort. Table 2 shows the values of all the elements utilized in the model. Bond graph simulation of a revolute joint between two consecutive links.

## 4.3 Bond graph modelling of revolute joints

The revolute joint can be modeled as a combination of rotational and linear couplings (Mishra & Vaz, 2017). In this work, revolute joints have been modeled using a combination of conditional rotational coupling (CRC) and translational coupling (TC) as illustrated in figure 7 and figure 8 respectively. The modelling of the revolute joint of the virtual subsystem hip_V and then the modelling of the revolute joint of the actual subsystem hip_A is discussed.

The revolute joint is a type of joint that allows rotation around a single axis. In the context of robotics, revolute joints are commonly used to connect two links in a robot arm. The rotational motion should be allowed about the $Z_{3V}$ axis only, and it should be constrained about the $X_{3V}$ and $Y_{3V}$ axes. The natural joints possess physiological damping due to the presence of the cartilage layer and the ligaments. Also, it is assumed that to achieve correct postures during sit-to-stand motion, the CNS learns to adjust the joint impedance as discussed by Soni & Vaz (2021). In model-V, both the physiological constraints and the constraints due to the nature of motion have been considered.

The modelling of the revolute joint is important because it allows us to simulate the behavior of the joint in different scenarios. For example, we can use the model to predict how the joint will behave under different loads or when subjected to different forces. This information can be used to optimize the design of the joint and ensure that it will perform as expected in real-world applications.

The natural joints possess physiological damping due to the presence of the cartilage layer and the ligaments. Further, it is assumed that to achieve correct posture during sit-to-stand movement, the CNS learns to adjust the impedance. In the model-V, a learned damping element R: $R_3$ is used to model the combined effect of physiological joint damping and the CNS learned impedance where $R_3 \in \mathbb{R}$. The CRC_Hip model is shown in figure 7. The angular velocities of Knee link and Hip link observed in the inertial frame {0} are represented by 1 junctions $1_0^0 \overline{\omega}_{Knee\_V}$ and $1_0^0 \overline{\omega}_{Hip\_V}$ , respectively. The relative angular velocity $_{Knee\_V}^{0} \overline{\omega}_{Hip\_V} = {}_0^0 \overline{\omega}_{Hip\_V} - {}_0^0 \overline{\omega}_{Knee\_V}$ of Hip link with respect to the Knee link and expressed in the inertial frame is calculated at $0_{\overline{\tau}_{Hip\_V}}$ junction. Then $\left[ _{Knee\_V}^{0} \overline{\omega}_{Hip\_V} \right]$ is expressed in the body frame {Hip_V} as $_{Knee\_V}^{Hip\_V} \overline{\omega}_{Hip\_V}$ using the modulated transformer $MTF: \left[ _{Hip\_V}^{0} R \right]$ as following:

$$_{Knee\_V}^{Hip\_V}\overline{\omega}_{Hip\_V} = \left[_{Hip\_V}^{0}R\right]^{T}{}_{Knee\_V}^{0}\overline{\omega}_{Hip\_V} \tag{13}$$

Further, $_{Knee\_V}^{Hip\_V}\overline{\omega}_{Hip\_V}$ is decomposed into three components as scalar bonds as shown in figure 9 in CRC2. Rotation about the $x_{Hip\_V}$ and $y_{Hip\_V}$ axes of the body frame is constrained using source of flow $Sf_{Knee\_Vx}:0$ and $Sf_{Knee\_Vy}:0$ respectively. The occurrence of derivative causality has been avoided by appropriately relaxing these constraints using viscoelastic couplings having torsional springs modelled as C and $C_1$, and dampers R and $R_1$ about the $x_{Hip\_V}$ and $y_{Hip\_V}$ axes respectively. Here C, $C_1$, R and R1 $\in \mathbb{R}$. The torque acting on Hip link about $x_{Hip\_V}$ and $y_{Hip\_V}$ axes of frame {Hip_V} are:

$$Hip\_V_{\tau_{Hip\_Vx}} = C \; _{Knee\_V}^{Hip\_V}\theta_{Hip\_Vx} + \; R \; _{Knee\_V}^{Hip\_V}\dot{\theta}_{Hip\_Vx} \tag{14}$$

$$Hip\_V_{\tau_{Hip\_Vy}} = C1 \; _{Knee\_V}^{Hip\_V}\theta_{Hip_{Vy}} + \; R1 \; _{Knee\_V}^{Hip\_V}\dot{\theta}_{Hip\_Vy} \tag{15}$$

Where $_{Knee\_V}^{Hip\_V}\dot{\theta}_{Hip\_Vx} = -\,_{Knee\_V}^{Hip\_V}\overline{\omega}_{Hip\_Vx}$ and $_{Knee\_V}^{Hip\_V}\dot{\theta}_{Hip_{Vy}} = -\,_{Knee\_V}^{Hip\_V}\overline{\omega}_{Hip\_Vy}$ are represented at junctions $1_{Knee\_V}^{Hip\_V}\dot{\theta}_{Hip\_Vx}$ and $1_{Knee\_V}^{Hip\_V}\dot{\theta}_{Hip\_Vy}$ respectively. Rotation about the $z_{Hip\_V}$ axis is permitted in a predefined region and beyond which it is restricted using a source of flow $Sf_{Knee\_Vz}:0$, a non-linear $C_2$ and $R_2$ elements. The characteristic functionality used here is already established in Pathak & Vaz (2020).

Let us consider joint angle for Knee joint, measured from $x_{Knee\_V}$ to $x_{Hip\_V}$, about $z_{Hip\_V}$ axis to be $_{Knee\_V}^{Hip\_V}\theta_{Hip\_Vz}$. For the modelling, let $_{Knee\_V}^{Hip\_V}\theta_{Hip\_Vz_{min}}$ and $_{Knee\_V}^{Hip\_V}\theta_{Hip\_Vz_{max}}$ is the allowed range of rotation for Knee joint or Hip-link. As long as the hip link rotates between $_{Knee\_V}^{Hip\_V}\theta_{Hip\_Vz_{min}}$ and $_{Knee\_V}^{Hip\_V}\theta_{Hip\_Vz_{max}}$, the non-linear elements $C_2$ and $R_2$ remain inactive. In the rotation region $_{Knee\_V}^{Hip\_V}\theta_{Hip\_Vz_{min}} \leq$ $_{Knee\_V}^{Hip\_V}\theta_{Hip_{Vz}} \leq \,_{Knee\_V}^{Hip\_V}\theta_{Hip\_Vz_{max}}$, the only torque due to the learned damping element R3 will act about the $z_{Hip\_V}$ axis of frame {Hip_V} as:

$$_{0}^{Hip\_V}\tau_{Hip\_Vz} = -R_3 \; _{Knee\_V}^{Hip\_V}\omega_{Hip\_Vz} \tag{16}$$

Where $_{Knee\_V}^{Hip\_V}\omega_{Hip\_Vz}$ is the component of angular velocity $_{Knee\_V}^{Hip\_V}\overline{\omega}_{Hip\_V}$ about the $z_{Hip\_V}$ direction.

As Hip link tries to go beyond either of the limits $_{Knee\_V}^{Hip\_V}\theta_{Hip\_Vz_{min}} \leq$ $_{Knee\_V}^{Hip\_V}\theta_{Hip\_Vz} \leq {}_{Knee\_V}^{Hip\_V}\theta_{Hip\_Vz\_max}$, the non-linear C2 and R2 elements become active. These elements represent a cushion to the limits of the rotation region. The angular deformation of the cushion is calculated as $_{Knee\_V}^{Hip\_V}\theta_{Hip\_Vz_d} = {}_{Knee\_V}^{Hip\_V}\theta_{Hip\_Vz} - {}_{Knee\_V}^{Hip\_V}\theta_{Hip\_Vz_{max}}$ when it transcends the maximum limit and $_{Knee\_V}^{Hip\_V}\theta_{Hip\_Vz_d} = {}_{Knee\_V}^{Hip\_V}\theta_{Hip\_Vz} - {}_{Knee\_V}^{Hip\_V}\theta_{Hip\_Vz_{min}}$ when it transcends the minimum limit.
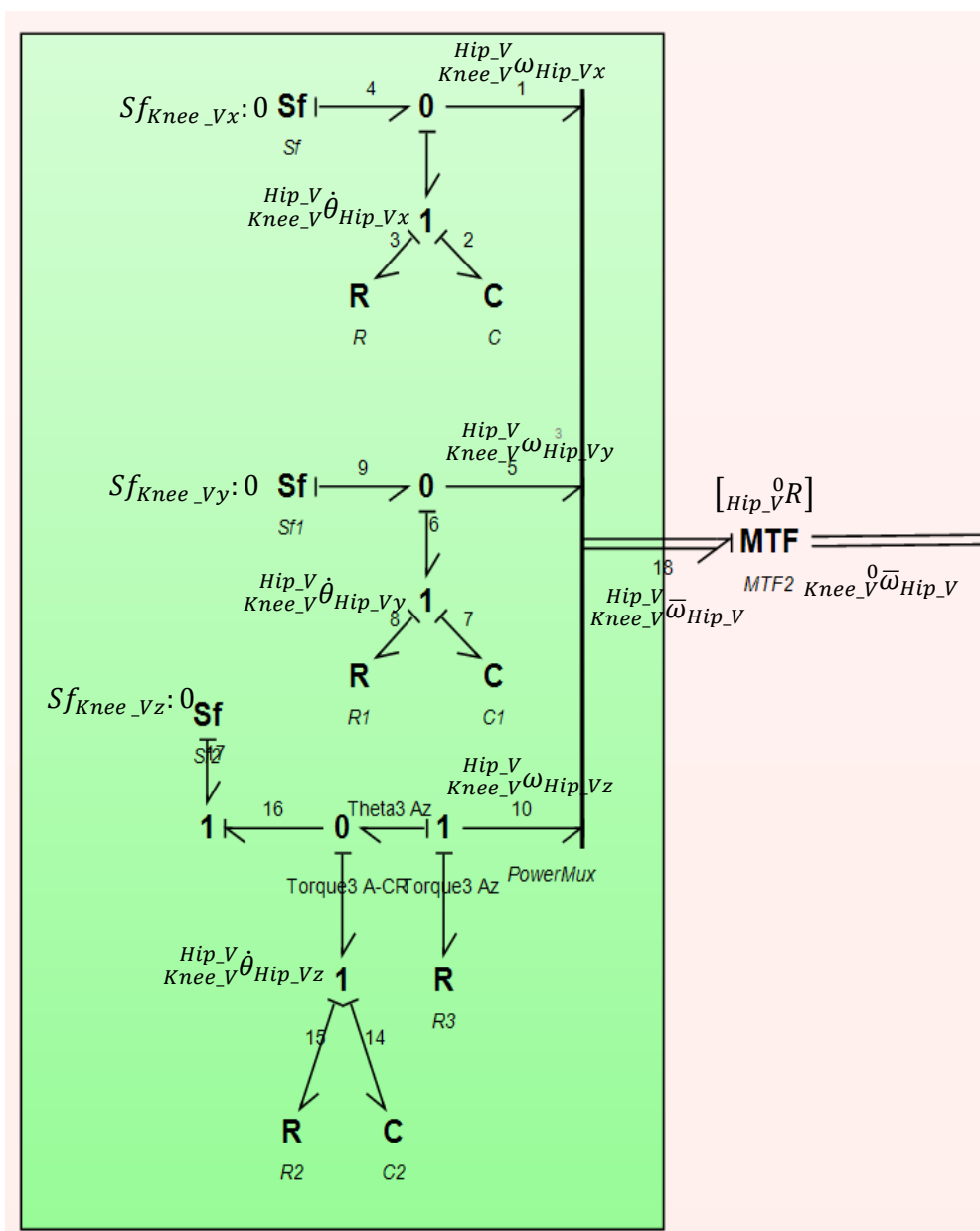


**Figure 7** Bond graph model of conditional rotational coupling

When $\quad {}^{Hip\_V}_{Knee\_V}\theta_{Hip\_Vz} = {}^{Hip\_V}_{Knee\_V}\theta_{Hip\_Vz_{max}} = {}^{Hip\_V}_{Knee\_V}\theta_{Hip\_Vz_{min}}$ then ${}^{Hip\_V}_{Knee\_V}\theta_{Hip\_Vz_d} = 0$. As the Hip-link transcends the maximum limit ${}^{Hip\_V}_{Knee\_V}\theta_{Hip\_Az} > {}^{Hip\_V}_{Knee\_V}\theta_{Hip\_Vz_{max}}$ and ${}^{Hip\_V}_{Knee\_V}\theta_{Hip\_Vz_d} \neq 0$, the non-linear elements will gradually start applying an opposing torque on Hip-link. The function of angular deformation of the cushion ${}^{Hip\_V}_{Knee\_V}\theta_{Hip\_Vz_d}$ represents the opposing torque as:

$${}^{Hip\_V}_{0}\tau_{Hip\_Vz} =$$

$$\begin{cases} -\left({}^{Hip\_V}_{0}\tau_{Hip\_Vz}\right)_{C2} - \left({}^{Hip\_V}_{0}\tau_{Hip\_Vz}\right)_{R2} - R_3 \, {}^{Hip\_V}_{Knee\_V}\omega_{Hip\_VZ} \; ; \; {}^{Hip\_V}_{Knee\_V}\omega_{Hip\_Vz} \geq 0 \\ -\left({}^{Hip\_V}_{0}\tau_{Hip\_Vz}\right)_{C2} - R_3 \, {}^{Hip\_V}_{Knee\_V}\omega_{Hip\_Vz} \qquad\qquad\quad ; \; {}^{Hip\_V}_{Knee\_V}\omega_{Hip\_Vz} < 0 \end{cases} \quad (17)$$
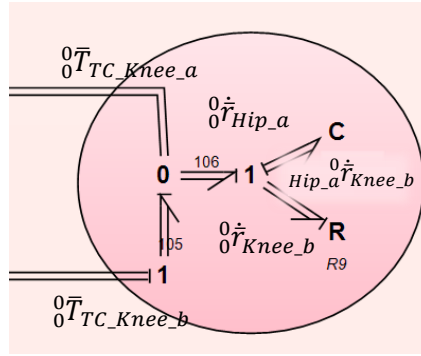


**Figure 8** Bond graph model of Translational Coupling

Similarly, if the Hip-link transcends the minimum limit ${}^{Hip\_V}_{Knee\_V}\theta_{Hip\_Vz} < {}^{Hip\_V}_{Knee\_V}\theta_{Hip\_Vz_{min}}$ and ${}^{Hip\_V}_{Knee\_V}\theta_{Hip\_Vz_d} \neq 0$, the opposing torque can be expressed as:

$${}^{Hip\_V}_{0}\tau_{Hip\_Vz} =$$

$$\begin{cases} -\left({}^{Hip\_V}_{0}\tau_{Hip\_Vz}\right)_{C2} - \left({}^{Hip\_V}_{0}\tau_{Hip\_Vz}\right)_{R2} - R_3 \, {}^{Hip\_V}_{Knee\_V}\omega_{Hip\_VZ} \; ; \; {}^{Hip\_V}_{Knee\_V}\omega_{Hip\_Vz} \leq 0 \\ -\left({}^{Hip\_V}_{0}\tau_{Hip\_Vz}\right)_{C2} - R_3 \, {}^{Hip\_V}_{Knee\_V}\omega_{Hip\_Vz} \qquad\qquad\quad ; \; {}^{Hip\_V}_{Knee\_V}\omega_{Hip\_Vz} > 0 \end{cases} \quad (18)$$

Where,

$$\left({}^{Hip\_V}_{0}\tau_{Hip\_Vz}\right)_{C2} =$$

$$C2 \left[ \frac{\left({}^{Hip\_V}_{Knee\_V}\theta_{Hip\_Vz_d}\right)^2}{\left({}^{Hip\_V}_{Knee\_V}\theta_{Hip\_Vz_{max}}\right)^2 \left(1 - \left(\frac{{}^{Hip\_V}_{Knee\_V}\theta_{Hip\_Vz_d}}{{}^{Hip\_V}_{Knee\_V}\theta_{Hip\_Vz_{max}}}\right)^2\right)} \right] sign\left({}^{Hip\_V}_{Knee\_V}\theta_{Hip\_Vz_d}\right) \qquad (19)$$

and,

$$\left(^{Hip_V}_{\ 0}\tau_{Hip_Vz}\right)_{R2} =$$

$$R2 \left[\frac{\left(^{Hip\_V}_{Knee\_V}\theta_{Hip\_Vz_d}\right)^2}{\left(^{Hip\_V}_{Knee\_V}\theta_{Hip\_Vz_{max}}\right)^2\left(1-\left(\frac{^{Hip\_V}_{Knee\_V}\theta_{Hip\_Vz_d}}{^{Hip\_V}_{Knee\_V}\theta_{Hip\_Vz_{max}}}\right)^2\right)}\right]^{Hip\_V}_{Knee\_V}\omega_{Hip\_Vz} \tag{20}$$

Where $C_2$ and $R_2$ are the positive constants such that $R_2$ and $C_2 \in \mathbb{R}$.

From (16) and (17), it can be noticed that when the Hip-link will try to deform the cushion on either of the limits, only then the nonlinear $C_2$ and $R_2$ elements are considered to acting and its velocity will be towards the limit. The $R_2$ element will be deactivated and the damping force will not act when the velocity of Hip-link is in the opposite direction to the limit and the cushion will be regaining its shape.

As the angular deformation of the cushion $^{Hip\_V}_{Knee\_V}\theta_{Hip\_Vz_d}$ tends to the maximum permissible angular deformation $^{Hip\_V}_{Knee\_V}\theta_{Hip\_Vz_{max}}$, the opposing torque by non-linear $C_2$ and $R_2$ elements in (18) and (19) tend to infinity. $^{Hip\_V}_{Knee\_V}\theta_{Hip\_Vz_{max}}$ is selected such that the Hip-link would never cross its natural limits of rotation during sit-to-stand motion. The net torque acting on Hip-joint due to the CRC$_2$ in the inertial frame {0} is represented as:

$$^0_0\bar{\tau}_{Hip\_V} = \left[_{Hip\_V}^{\ 0}R\right]^{Hip\_V}\bar{\tau}_{Hip\_V} \tag{21}$$

$Where\ ^{Hip\_V}\bar{\tau}_{Hip\_V} = \{\ ^{Hip\_V}\bar{\tau}_{Hip\_Vx}\ ,\ ^{Hip\_V}\bar{\tau}_{Hip\_Vy}\ ,\ ^{Hip\_V}\bar{\tau}_{Hip\_Vz}\ \}^T.$

The bond graph of TC$_2$ and CRC$_2$ between Hip and Knee is shown in figure 9. Similar approach is used when modelling bond graph of TC$_1$ and CRC$_1$ between Knee and Ankle, and modelling bond graph of TC$_3$ and CRC$_3$ between HAT and Hip.

The modelling of the revolute joint of the model-A Hip_A, Knee_A and Ankle-A is similar to that of the model-V with few exceptions. One difference is that in model-A, only the physiological constraints of joint motion have been taken into consideration. The second difference is that in the model-A, only the physiological joint damping has been considered using a physiological damping element R$_{29}$. The TC$_1$, TC$_2$ and TC$_3$ of model-V and TC$_1$, TC$_2$ and TC$_3$ of model-A are similar to each other. The torque acting on Hip-

link about the $x_{Hip\_A}$ and $y_{Hip\_A}$ axes of frame {Hip_A} are formulated similarly for the model-V.
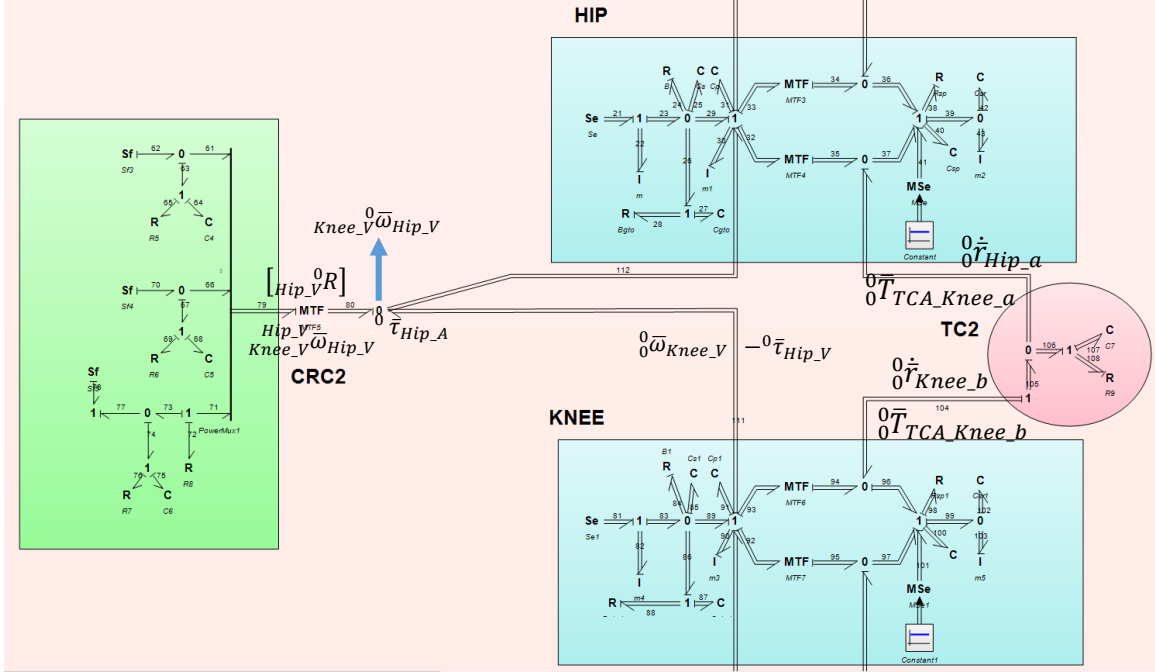


**Figure 9** Bond graph model of revolute joints between links. This shows connections of rotational and translational coupling between hip and knee joints.

$$^{Hip_A}\bar{\tau}_{Hip_{Ax}} = C_{Knee\_A}\ {}^{Hip\_V}_{Knee\_V}\theta_{Hip\_Ax} + R_{Knee\_A}\ {}^{Hip\_V}_{Knee\_V}\theta_{Hip\_Ax} \tag{22}$$

$$^{Hip_A}\bar{\tau}_{Hip_{Ay}} = C_{Knee\_A}\ {}^{Hip\_V}_{Knee\_V}\theta_{Hip\_Ay} + R_{Knee\_A}\ {}^{Hip\_V}_{Knee\_V}\theta_{Hip\_Ay} \tag{23}$$

## 4.4 Bond graph modelling of a ground link

In both the actual and virtual subsystems, it is assumed that there is enough friction between the feet and the ground in the $x_0$ and $z_0$ directions. As a result, any movement of the feet in the $x_0$ and $z_0$ directions is prohibited. Furthermore, in normal sit-to-stand and stand-to-sit motions, the feet do not lose contact with the ground. The human body would do so by exerting force on the earth. Some of the muscles in the lower limbs would provide this force. The restriction of motion of feet in the $y_0$ direction is achieved by restricting their motion in the $y_0$ direction as well. This can be understood as if the muscles

of the shanks and feet generate the necessary forces to keep the feet in contact with the ground during sit-to-stand and stand-to-sit motions.
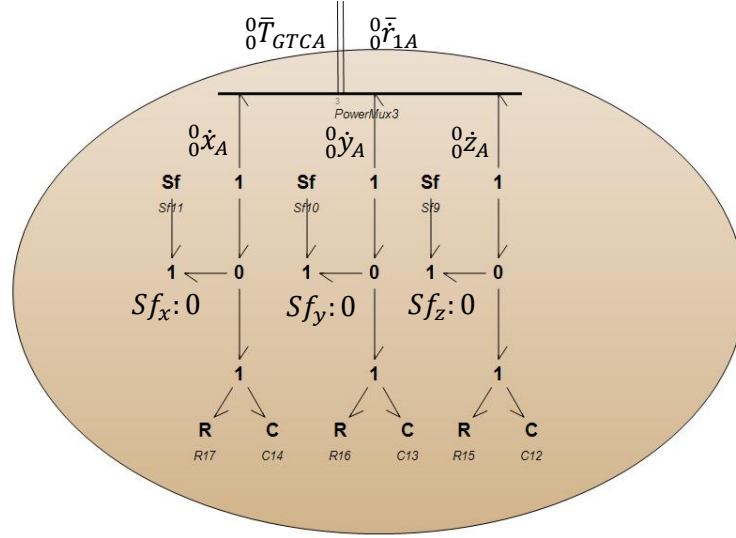


**Figure 10** Bond graph model of ground structure: GTC$_A$.

For the actual subsystem, only one point on the ground 'GTC$_A$' is taken into account. There is additionally one viscoelastic coupling: GTC$_A$ between points ground and ankle joint connection in this scenario. Figure 11 depicts the GTC$_A$ bond graph structure. GTC$_V$'s bond graph structure is comparable to that of GTC$_A$. As illustrated in figure 11, movement is restricted in x0, y0 and z0 direction and have been constrained using source of flow elements; Sf=0, linear stiffness elements; C$_{12}$, C$_{13}$ and C$_{14}$, damping elements; R$_{15}$, R$_{16}$ and R$_{17}$ respectively. Here all values of linear stiffness elements and damping elements $\in \mathbb{R}$. The effort by the coupling of GTC$_A$ on ankle joint link will be:

$$\bar{T}_{GTCA} = \begin{Bmatrix} C_{14} \, {}^0_{gA}x_A + R_{17} \, {}^0_{gA}\dot{x}_A \\ C_{13} \, {}^0_{gA}y_A + R_{16} \, {}^0_{gA}\dot{y}_A \\ C_{12} \, {}^0_{gA}z_A + R_{15} \, {}^0_{gA}\dot{z}_A \end{Bmatrix} \tag{24}$$

Where ${}^0_{gA}x_A$, ${}^0_{gA}y_A$ and ${}^0_{gA}z_A$ are the relative positions of point ankle-joint on ankle-joint to a point g$_A$ on the ground. ${}^0_{gA}\dot{x}_A$, ${}^0_{gA}\dot{y}_A$ and ${}^0_{gA}\dot{z}_A$ are the relative velocities.

Similarly, $\bar{T}_{GTCV}$ have been derived. Similar couplings $gTC_v$ have been used for modelling of ground in the model-V. Forces by the model-V are derived as done for the couplings of the actual system given in (25).

$$\bar{T}_{GTCV} = \begin{Bmatrix} C_{21}\ {}_{gA}^{0}x_A + R_{27}\ {}_{gA}^{0}\dot{x}_A \\ C_{20}\ {}_{gA}^{0}y_A + R_{26}\ {}_{gA}^{0}\dot{y}_A \\ C_{19}\ {}_{gA}^{0}z_A + R_{25}\ {}_{gA}^{0}\dot{z}_A \end{Bmatrix} \tag{25}$$

**4.5 Bond graph modelling of PID controller**

The focus is on refining the control systems to accommodate the nonlinear characteristics of the integrated muscle models. Key aspects include:

- Controller Tuning: The Proportional-Integral-Derivative (PID) controllers are fine-tuned to align with the nonlinear response of muscles as represented by the Hill-type models. This involves adjusting the PID parameters to achieve desired dynamic responses during joint movements.

- Response Calibration: The controllers are calibrated to ensure that the muscle response under various load and speed conditions is accurately reflected. This calibration is crucial for replicating realistic joint movements in simulations.

- Integration with Muscle Dynamics: The adapted control mechanisms are integrated with the muscle dynamics to create a cohesive system. This ensures that the control response is harmoniously synchronized with muscle force generation and joint dynamics.

- Simulation Testing: Preliminary testing of the adapted control systems is conducted through simulations to validate their performance. Adjustments are made based on these tests to optimize the control response.

By adapting the control mechanisms in this manner, the methodology ensures that the model accurately captures the complex interplay between muscle forces and joint movements.

About the $z_{Hip\_A}$ axis of the frame {Hip_A}, an additional torque $\left({}^{Hip_A}\tau_{Hip_A}\right)_{CR}$ from the BGM of PID$_3$ to the BGM of CRC$_{3A}$ acts on the Hip-link as shown in figure 11. Based on the error $\varepsilon_{Hip\_A} = {}_{Knee\_V}^{Hip\_V}\theta_{Hip\_Vz} - {}_{Knee\_A}^{Hip\_A}\theta_{Hip\_Az}$ between the desired joint angle ${}_{Knee\_V}^{Hip\_V}\theta_{Hip\_Vz}$ to the actual joint angle ${}_{Knee\_A}^{Hip\_A}\theta_{Hip\_Az}$, the PID$_3$ controller would

generate the necessary torque $\left( {}^{HipA}\tau_{HipA} \right)_{CR}$ to be applied at the revolute Hip-joint of the model-A. Here, it can be seen that the model-V (CNS) determines the desired joint angle ${}^{Hip\_V}_{Knee\_V}\theta_{Hip\_Vz}$ by taking into account the joint limits including both physiological limits and limits due to the nature.

Furthermore, to achieve the desired joint angle ${}^{Hip\_V}_{Knee\_V}\theta_{Hip\_Vz}$, the PID-controller of the Hip-Joint would generate a joint torque such that Hip-link would never transcend the joint limits. When the PID-controller which mimics the function of muscle is not working then the physiological limits modelled in the model-A acts to stop the movement of the links. The elements are represented by C for proportional gain, Se for integral gain and R for derivative gain.

$$C = C_{P\_Hip\_A}\,\varepsilon_{Hip\_A} \tag{26}$$

$$R = R_{D\_Hip\_A}\,\varepsilon_{Hip\_A} \tag{27}$$

$$Se = C_{I\_Hip\_A}\int_{\tau=t_i}^{t}\varepsilon_{Hip\_A}(\tau)\,d\tau \tag{28}$$

In the same manner, PID-controllers are used for all the joints i.e. Knee and Ankle. For the actual subsystem, when Hip-link rotates between the maximum and minimum limits of rotation ${}^{Hip\_A}_{Knee\_A}\theta_{Hip\_Az_{min}} \leq {}^{Hip\_A}_{Knee\_A}\theta_{Hip\_Az} \leq {}^{Hip\_A}_{Knee\_A}\theta_{Hip\_Az_{max}}$, the torque acting on it can be given as:

$$^{HipA}\tau_{HipA} = \left( {}^{HipA}\tau_{HipA} \right)_{CR} - R_2\,{}^{Hip\_V}_{Knee\_V}\omega_{Hip\_Vz} \tag{29}$$

When Hip_A link tries to go beyond the maximum limit of rotation ${}^{Hip\_A}_{Knee\_A}\theta_{Hip\_Az} > {}^{Hip\_A}_{Knee\_A}\theta_{Hip\_Az_{max}}$ then the torque acting on it can be represented as:

$$^{HipA}_{0}\tau_{Hip_{Az}} =$$

$$\begin{cases} \left( {}^{HipA}\tau_{HipA} \right)_{CR} - \left( {}^{Hip\_A}_{0}\tau_{Hip\_Az} \right)_{C2} - \left( {}^{Hip\_A}_{0}\tau_{Hip\_Az} \right)_{R2} - R_2\,{}^{Hip\_A}_{Knee\_A}\omega_{Hip\_AZ} \;;\; {}^{Hip\_A}_{Knee\_A}\omega_{Hip\_Az} \geq 0 \\[2ex] \left( {}^{HipA}\tau_{HipA} \right)_{CR} - \left( {}^{Hip\_A}_{0}\tau_{Hip\_Az} \right)_{C2} - R_2\,{}^{Hip\_A}_{Knee\_A}\omega_{Hip\_Az} \qquad\qquad\;;\; {}^{Hip\_A}_{Knee\_A}\omega_{Hip\_Az} < 0 \end{cases}$$

$$\tag{30}$$

Similarly, if the Hip-link transcends the minimum limit ${}^{Hip\_A}_{Knee\_A}\theta_{Hip\_Az} < {}^{Hip\_A}_{Knee\_A}\theta_{Hip\_Az_{min}}$, the torque acting on it can be expressed as:

$$^{Hip_A}_{\quad 0}\tau_{Hip_{Az}} =$$

$$\begin{cases} \left(^{Hip_A}\tau_{Hip_A}\right)_{CR} - \left(^{Hip\_A}_{\quad 0}\tau_{Hip\_Az}\right)_{C2} - \left(^{Hip\_A}_{\quad 0}\tau_{Hip\_Az}\right)_{R2} - R_2 \,^{Hip\_A}_{Knee\_A}\omega_{Hip\_AZ} \;;\; ^{Hip\_A}_{Knee\_A}\omega_{Hip\_Az} \le 0 \\ \left(^{Hip_A}\tau_{Hip_A}\right)_{CR} - \left(^{Hip\_A}_{\quad 0}\tau_{Hip\_Az}\right)_{C2} - R_2 \,^{Hip\_A}_{Knee\_A}\omega_{Hip\_Az} \qquad\qquad\qquad\;;\; ^{Hip\_A}_{Knee\_A}\omega_{Hip\_Az} > 0 \end{cases}$$

$$(31)$$

Where

$$\left(^{Hip_A}\tau_{Hip_A}\right)_{CR} = R + C + Se \tag{32}$$

Which has already been established in (26)-(28).

The power generated by the PID-controller is:

$$\left(P_{Hip\_A}\right)_{CR} = \left(^{Hip_A}\tau_{Hip_A}\right)_{CR} \,^{Hip\_A}_{Knee\_A}\omega_{Hip\_Az} \tag{33}$$

The net power given to Hip-joint is:

$$P_{Hip\_A} = \,^{Hip_A}\tau_{Hip_A} \,^{Hip\_A}_{Knee\_A}\omega_{Hip\_Az} \tag{34}$$

The net torque acting on the Hip-link in the inertial frame {0} is:

$$^{0}_{0}\bar{\tau}_{Hip_A} = \left[^{0}_{Hip\_A}R\right] \,^{Hip\_A}\bar{\tau}_{Hip\_A} \tag{35}$$

*Where* $^{Hip\_A}\bar{\tau}_{Hip\_A} = \{\,^{Hip\_A}\bar{\tau}_{Hip\_Ax}\,,\,^{Hip\_A}\bar{\tau}_{Hip\_Ay}\,,\,^{Hip\_A}\bar{\tau}_{Hip\_Az}\,\}^{T}$.
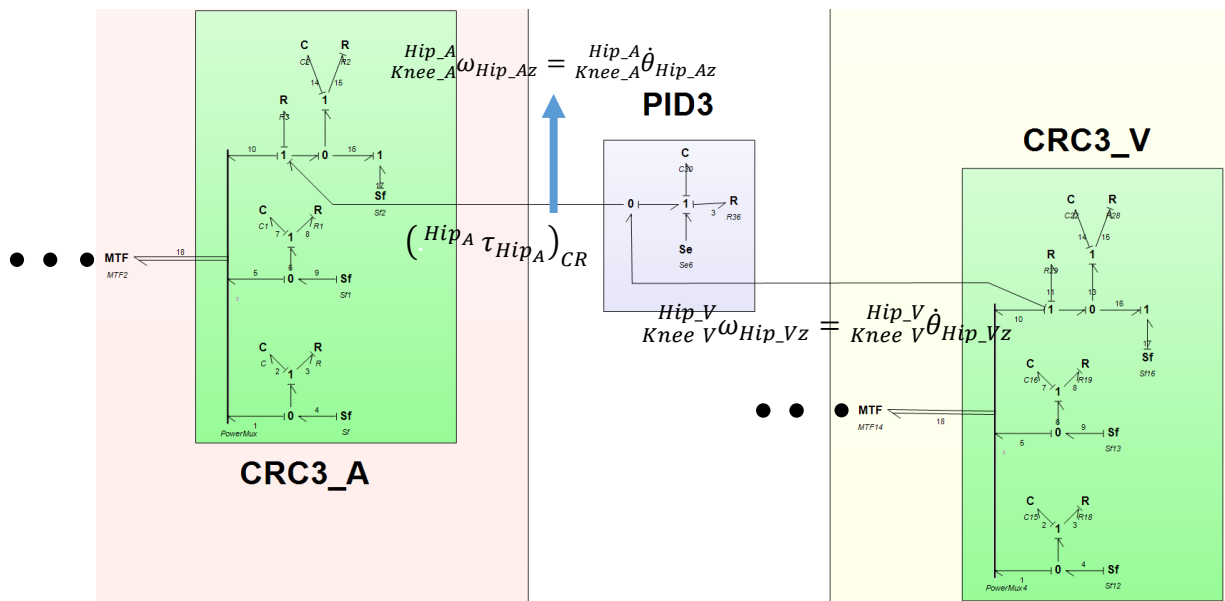


**Figure 11** Bond graph model of PID controller between Model-A and Model-V.

## 4.6 Bond graph modelling of model-V

Complete bond graph model of the model-V is given in figure 13. The links are represented as BGM of HAT, Hip, Knee and Ankle. The revolute joints between the links are represented as BGM of $CRC_i$ and $TC_i$, where i=1,..,3. The force of gravity is also considered by imposing an effort using $Se: \begin{matrix} 0 \\ -M_{link}g \\ 0 \end{matrix}$ at the center of mass of each link, where $link = HAT, Hip, Knee$ and $Ankle$.

For the virtual model, the position of center of mass of all links can be derived as:

$$_0^0\bar{r}_{COM\_V} = \frac{\sum_{i=1}^{4} M_{iV} \, _0^0\bar{r}_{iVC}}{\sum_{i=1}^{4} M_{iV}} \tag{36}$$

And by differentiating (36), we get:

$$_0^0\dot{\bar{r}}_{COM\_V} = \frac{\sum_{i=1}^{4} M_{iV} \, _0^0\dot{\bar{r}}_{iVC}}{\sum_{i=1}^{4} M_{iV}} \tag{37}$$

This can also be re-written as:

$$_0^0\dot{\bar{r}}_{COM\_V} = \frac{M_{HAT\_V} \, _0^0\dot{\bar{r}}_{HAT\_VC}}{\sum_{i=1}^{4} M_{iV}} + \frac{M_{Hip\_V} \, _0^0\dot{\bar{r}}_{Hip\_VC}}{\sum_{i=1}^{4} M_{iV}} + \frac{M_{Knee\_V} \, _0^0\dot{\bar{r}}_{Knee\_VC}}{\sum_{i=1}^{4} M_{iV}} + \frac{M_{Ankle\_V} \, _0^0\dot{\bar{r}}_{Ankle\_VC}}{\sum_{i=1}^{4} M_{iV}}$$
$$\tag{38}$$

Similarly, the position of combined center of mass of the model-A is derived. As illustrated in figure 13, the trajectory of the COMB is being fed to the COM_V of the model-V as a vector source of the flow $= \begin{Bmatrix} _0^0\dot{x}_{COMB} \\ _0^0\dot{y}_{COMB} \\ 0 \end{Bmatrix}$.
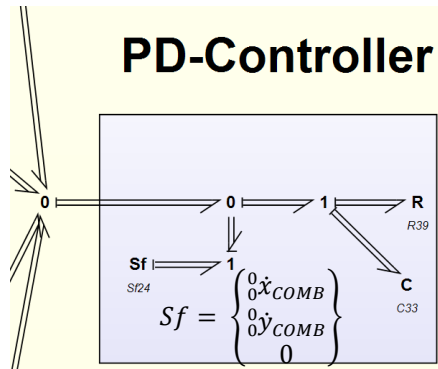


**Figure 12** Bond graph model of PD-controller.

Where $_0^0\dot{x}_{COMB}$ and $_0^0\dot{y}_{COMB}$ are the first derivatives of the piece-wise mapped time polynomials as established in Soni & Vaz (2021). $_0^0\dot{x}_{COMB}$ and $_0^0\dot{y}_{COMB}$ are the imposed flow trajectories in the $x_0$ and $y_0$ directions, respectively. By imposing 0 flow, any motion in the $z_0$ direction is restricted. The sub-model of PD-controller as illustrated in figure 13 is used to apply the required amount of effort on the COM_V of the model-V to move it along the desired trajectory of the COMB. The joint rate trajectories of the respective joints are taken as outputs from model-V.

An important aspect can be noted that the velocity of the $COM\_V$ $_0^0\dot{r}_{COM\_V}$ is obtained (38) using the velocity of the center of mass of each link from Figure 12. The effort that is required to be applied at the center of masse of each link is found to be distributed in the same proportion given by the TF elements used to connect links with PD-Controller. This insight is drawn based on the graphical representation of causality in the bond graph structure of model-V.

### 4.7 Bond graph modelling of model-A

The model-A of the actual subsystem for sit-to-stand motion is shown in figure 14. Similar to actual model the revolute joints are represented as $CRC_i$ and $TC_i$, where i=1,..,3. HAT, Hip, Knee, Ankle and ground are also represented in figure 14.

The joint rate trajectories from the model-V are input to the PID-controller at the respective joints of the model-A. The PID-controller of the respective joint applies the desired torque on the joint of the model-A, based on the error between the desired and actual angles. The resultant desired torque is such that it tracks the desired joint trajectory of model-V. Eventually it follows the desired trajectory of COMB by COM_A tracking the motion of COM_V.
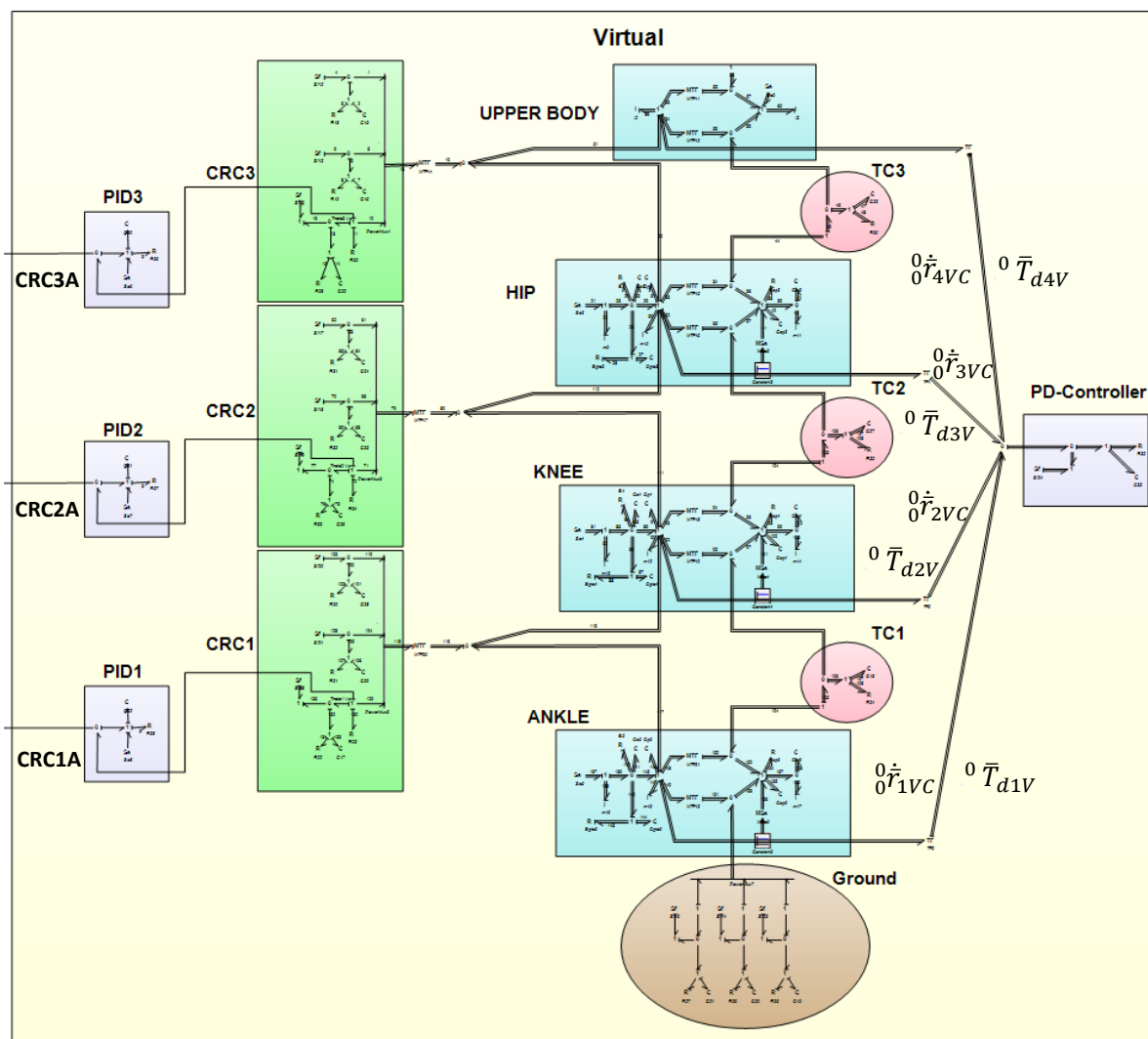
**Figure 13** Bond graph model of Model-V
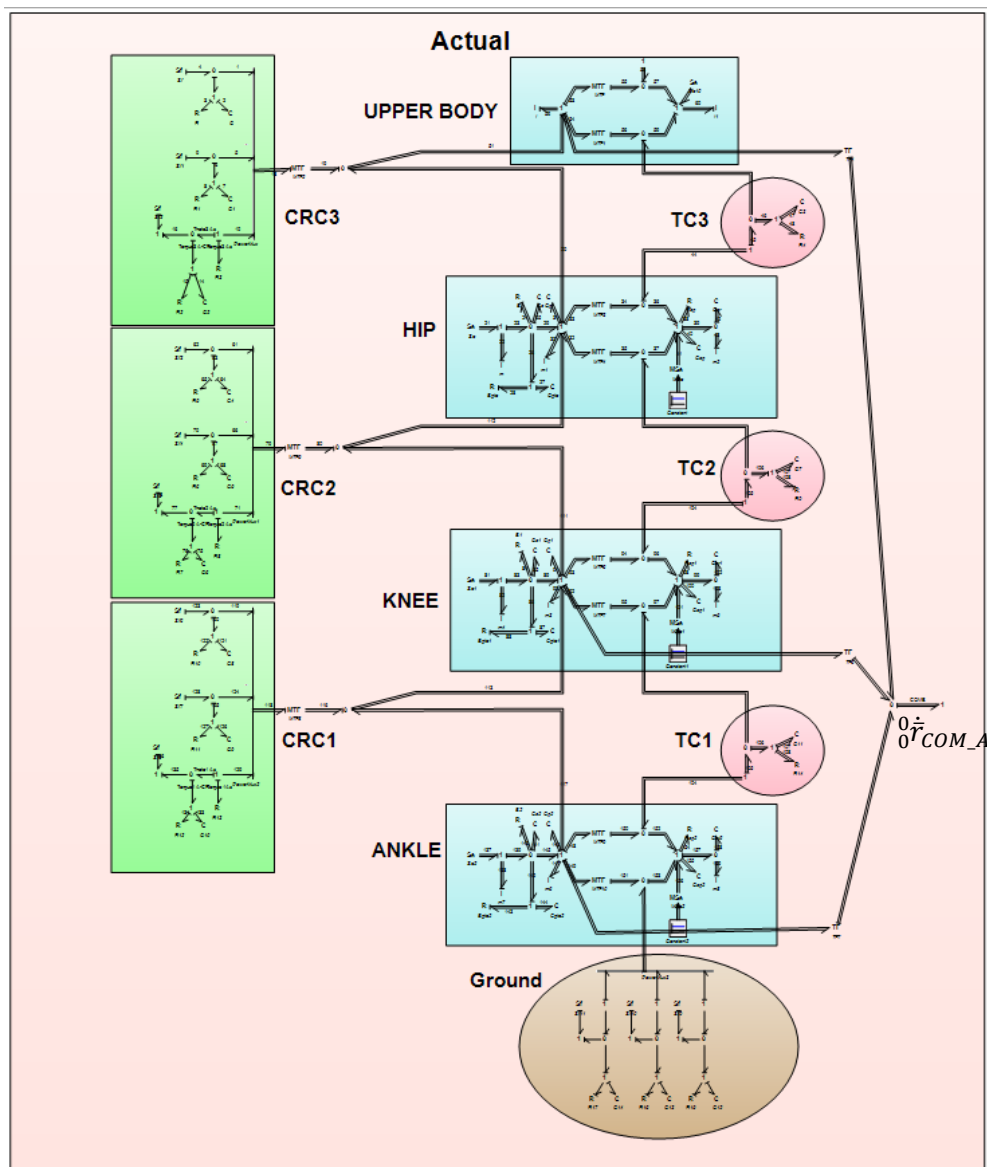
**Figure 14** Bond graph model of Model-A

# CHAPTER 5

# SYSTEM EQUATIONS

Model equations governing the dynamics of sit-to-stand motion are systematically derived from the bond graph models. The equations for rate of change of translational momentum and rate of change of angular momentum are derived for both Model-A and Model-V.

## 5.1 Translational dynamics for the model-A

For ankle joint,

$$\frac{dy}{dx}{}^0\overline{X_{Ankle}} = \ \bar{T}_{GTCA} + \left[-\bar{T}_{TC\_ankle}\right] + \begin{Bmatrix} 0 \\ -M_{ankle}g \\ 0 \end{Bmatrix} \tag{39}$$

Where $\overline{X_{Ankle}}$ is the translational momentum of ankle joint, expressed in the inertial frame $\{0\}$. $\bar{T}_{gTCA}$ is a reaction force due to gTC$_A$ as given in (23) and $\bar{T}_{TC\_ankle}$ is the reaction force by TC$_{A\_ankle.}$

$$\bar{T}_{TC\_ankle} = \ \left[C_{Knee\_A}\right] {}_{2A}^{0}\bar{r}_{1Ab} + \ \left[R_{Knee\_A}\right] {}_{2A}^{0}\bar{r}_{1Ab} \tag{40}$$

Where ${}_{2A}^{0}\bar{r}_{1Ab} = \ {}_{0}^{0}\bar{r}_{1Ab} - \ {}_{0}^{0}\bar{r}_{2Aa}$ is expressed in the frame $\{0\}$ and is the relative position of point $1A_b$ with respect to point $2A_a$. The relative velocity of point $1A_b$ is given by ${}_{2A}^{0}\dot{\bar{r}}_{1Ab} = \ {}_{0}^{0}\dot{\bar{r}}_{1Ab} - \ {}_{0}^{0}\dot{\bar{r}}_{2Aa}$ with respect to point $2A_a$. Similarly the reaction forces $\bar{T}_{TC\_hip}$ and $\bar{T}_{TC\_knee}$ due to the TC$_{A\_hip\ and}$ TC$_{A\_knee}$ are calculated respectively.

For knee joint,

$$\frac{d}{dx}{}^0\overline{X_{knee}} = \ \bar{T}_{TC\_ankle} + \left[-\bar{T}_{TC\_knee}\right] + \begin{Bmatrix} 0 \\ -M_{knee}g \\ 0 \end{Bmatrix} \tag{41}$$

For hip joint,

$$\frac{d}{dx} {}^0\overline{x_{hip}} = \overline{T}_{TC\_knee} + \left[-\overline{T}_{TC\_hip}\right] + \begin{Bmatrix} 0 \\ -M_{hip}g \\ 0 \end{Bmatrix} \tag{42}$$

For upper body i.e. head-arm-trunk (HAT),

$$\frac{d}{dx} {}^0\overline{x_{HAT}} = \overline{T}_{TC\_hip} + \begin{Bmatrix} 0 \\ -M_{HAT}g \\ 0 \end{Bmatrix} \tag{43}$$

## 5.2 Translational dynamics for the model-V

The equations for the rate of change of momentum of model-V are similar as of model-A except for an additional term ${}^0\overline{T}_{diV}$ in each equation due to the PD-controller.

$$ {}^0\overline{T}_{diV} = [N_{iv}] \, {}^0\overline{T}_d \tag{44}$$

Where $[N_{iv}]$ is the modulus of the transformer for each link as derived in (38). ${}^0\overline{T}_d$ is the force by the PD-controller.

$$ {}^0\overline{T}_d = [C_P] \, \bar{\varepsilon}_{COMB} + [R_D] \, \dot{\bar{\varepsilon}}_{COMB} \tag{45}$$

Where $\bar{\varepsilon}_{COMB} = \left\{ {}^0_0\bar{r}_{COMB\_V} - {}^0_0\bar{r}_{COMB\_d} \right\}$, is the position error between the position of COM_V and the desired position of COMB. The velocity error between the velocity of COM_V and COMB is represented by $\dot{\bar{\varepsilon}}_{COMB} = \left\{ {}^0_0\dot{\bar{r}}_{COM\_V} - {}^0_0\dot{\bar{r}}_{COMB\_d} \right\}$. Hence for Ankle link,

$$\frac{d}{dx} {}^0\overline{x_{Ankle}} = \overline{T}_{GTC} + \left[-\overline{T}_{TC\_Ankle}\right] + {}^0\overline{T}_{d1V} + \begin{Bmatrix} 0 \\ -M_{Ankle}g \\ 0 \end{Bmatrix} \tag{46}$$

For Knee link,

$$\frac{d}{dx} {}^0\overline{x_{Knee}} = \overline{T}_{TC\_Ankle} + \left[-\overline{T}_{TC\_Knee}\right] + {}^0\overline{T}_{d2V} + \begin{Bmatrix} 0 \\ -M_{Knee}g \\ 0 \end{Bmatrix} \tag{47}$$

For Hip link,

$$\frac{d}{dx} {}^0\overline{x_{Hip}} = \overline{T}_{TC\_Hip} + \left[-\overline{T}_{TC\_Knee}\right] + {}^0\overline{T}_{d3V} + \begin{Bmatrix} 0 \\ -M_{Hip}g \\ 0 \end{Bmatrix} \tag{48}$$

For HAT link,

$$\frac{d}{dx} {}^{0}\overline{x}_{HAT} = \overline{T}_{TC_{HAT}} + \overline{T}_{TC_{Hip}} + \left[-\overline{T}_{TC\_Ankle}\right] + {}^{0}\overline{T}_{d1V} + \begin{Bmatrix} 0 \\ -M_{HAT}g \\ 0 \end{Bmatrix} \quad (49)$$

The velocities of center of masses of links of the model-V are formulated the same way as for the model-A.

## 5.3 Rotational dynamics for the model-A

For Ankle link,

$$\frac{d}{dx} {}_{Ankle_{Ac}}{}^{0}\overline{q}_{Ankle} = -{}^{0}\overline{\tau}_{Knee\_A} + \left[{}_{Ankle\_Ac}{}^{0}\overline{r}_{Ankle\_Aa} \times\right]\overline{T}_{GTC} +$$

$$\left[{}_{Ankle\_Ac}{}^{0}\overline{r}_{Ankle\_Ab} \times\right]\left\{-\overline{T}_{TC\_Ankle}\right\} \quad (50)$$

Where ${}_{Ankle_{Ac}}{}^{0}\overline{q}_{Ankle}$ is the angular momentum of Ankle link with respect to it's center of mass and expressed in frame {0}. ${}^{0}\overline{\tau}_{Knee\_A}$ is the reaction torque acting on ankle link by CRC1. $\left[{}_{Ankle\_Ac}{}^{0}\overline{r}_{Ankle\_Aa} \times\right]\overline{T}_{GTC}$ and $\left[{}_{Ankle\_Ac}{}^{0}\overline{r}_{Ankle\_Ab} \times\right]\overline{T}_{TC\_Ankle}$ are moments about the center of mass of ankle link exerted due to forces $\overline{T}_{GTC}$ and $\overline{T}_{TC\_Ankle}$ respectively.

For Knee link,

$$\frac{d}{dx} {}_{Knee_{Ac}}{}^{0}\overline{q}_{Knee} = {}^{0}\overline{\tau}_{Knee\_A} - {}^{0}\overline{\tau}_{Hip\_A} + \left[{}_{Knee\_Ac}{}^{0}\overline{r}_{Knee\_Aa} \times\right]\overline{T}_{TC\_Ankle} +$$

$$\left[{}_{Knee\_Ac}{}^{0}\overline{r}_{Knee\_Ab} \times\right]\left\{-\overline{T}_{TC\_Knee}\right\} \quad (51)$$

Where ${}^{0}\overline{\tau}_{Hip\_A}$ is the reaction torque acting on Ankle link by CRC2 as established in (20). Similarly, ${}^{0}\overline{\tau}_{Knee\_A}$, ${}^{0}\overline{\tau}_{Ankle\_A}$ and ${}^{0}\overline{\tau}_{HAT\_A}$ have been derived.

For Hip link,

$$\frac{d}{dx} {}_{Hip_{Ac}}{}^{0}\overline{q}_{Hip} = {}^{0}\overline{\tau}_{Hip\_A} - {}^{0}\overline{\tau}_{HAT\_A} + \left[{}_{Hip\_Ac}{}^{0}\overline{r}_{Hip\_Aa} \times\right]\overline{T}_{TC\_Hip} +$$

$$\left[{}_{Hip\_Ac}{}^{0}\overline{r}_{Hip\_Ab} \times\right]\overline{T}_{Knee\_Ab} \quad (52)$$

For HAT link,

$$\frac{d}{dx} {}_{HAT_{Ac}}{}^{0}\overline{q}_{HAT} = {}^{0}\overline{\tau}_{HAT\_Aa} + {}^{0}\overline{\tau}_{HAT\_Ab} + \left[{}_{HAT\_Ac}{}^{0}\overline{r}_{HAT\_Aa} \times\right]\overline{T}_{TC\_Hip} +$$

$$\left[{}_{HAT\_Ac}{}^{0}\overline{r}_{HAT\_Ab} \times\right]\overline{T}_{TC\_HAT} \quad (53)$$

The angular velocity for each link for model-A can be derived as:

$$ {}^{0}_{0}\bar{\omega}_{link} = \left[ {}_{link_{AC}}{}^{0}I_{link\_A} \right]^{-1} {}_{link_{AC}}{}^{0}\bar{q}_{link} \tag{54}$$

Where $link = HAT, Hip, Knee \ and \ Ankle$ of the actual model.

## 5.4 Rotational dynamics for the model-V

Rotational dynamics for model-V are similar to that of model-A.

For Ankle link,

$$ \frac{d}{dx} {}_{Ankle_{Vc}}{}^{0}\bar{q}_{Ankle} = -{}^{0}\bar{\tau}_{Knee\_V} + \left[ {}_{Ankle\_Vc}{}^{0}\bar{r}_{Ankle\_Va} \times \right] \bar{T}_{GTC} + $$
$$ \left[ {}_{Ankle\_Vc}{}^{0}\bar{r}_{Ankle\_Vb} \times \right]\left\{ -\bar{T}_{TC\_Ankle} \right\} \tag{55}$$

For Knee link,

$$ \frac{d}{dx} {}_{Knee_{Vc}}{}^{0}\bar{q}_{Knee} = {}^{0}\bar{\tau}_{Knee\_V} - {}^{0}\bar{\tau}_{Hip\_V} + \left[ {}_{Knee\_Vc}{}^{0}\bar{r}_{Knee\_Va} \times \right] \bar{T}_{TC\_Ankle} + $$
$$ \left[ {}_{Knee\_Vc}{}^{0}\bar{r}_{Knee\_Vb} \times \right]\left\{ -\bar{T}_{TC\_Knee} \right\} \tag{56}$$

For Hip link,

$$ \frac{d}{dx} {}_{Hip_{Vc}}{}^{0}\bar{q}_{Hip} = {}^{0}\bar{\tau}_{Hip\_V} - {}^{0}\bar{\tau}_{HAT\_V} + \left[ {}_{Hip\_Vc}{}^{0}\bar{r}_{Hip\_Va} \times \right] \bar{T}_{TC\_Hip} + $$
$$ \left[ {}_{Hip\_Vc}{}^{0}\bar{r}_{Hip\_Vb} \times \right] \bar{T}_{Knee\_Vb} \tag{57}$$

For HAT link,

$$ \frac{d}{dx} {}_{HAT_{Vc}}{}^{0}\bar{q}_{HAT} = {}^{0}\bar{\tau}_{HAT\_Va} + {}^{0}\bar{\tau}_{HAT\_Vb} + \left[ {}_{HAT\_Vc}{}^{0}\bar{r}_{HAT\_Va} \times \right] \bar{T}_{TC\_Hip} + $$
$$ \left[ {}_{HAT\_Vc}{}^{0}\bar{r}_{HAT\_Vb} \times \right] \bar{T}_{TC\_HAT} \tag{58}$$

The angular velocity for each link for model-V can be derived as:

$$ {}^{0}_{0}\bar{\omega}_{link} = \left[ {}_{link_{VC}}{}^{0}I_{link\_V} \right]^{-1} {}_{link_{VC}}{}^{0}\bar{q}_{link} \tag{59}$$

Where $link = HAT, Hip, Knee \ and \ Ankle$ of the virtual model.

**CHAPTER 6**

**RESULTS AND DISCUSSION**

This section explains the simulation results along with parameters and initial conditions taken for the simulation. Simulations are performed to analyze the dynamics of sit-to-stand motion of human being using the developed BGM. Simulations are done in 20-SIM for the developed BGM.

**6.1 Parameters and conditions**

The mass, length, moments of inertia and products of inertia of HAT-link of the model-A is taken from Soni & Vaz (2021). Table 1 shows the parameters of anthropometric properties of human body.

These properties are same for both model-A and model-V. Total time to complete one stand-to-sit moment is $t = 4.87 - 1.76 = 3.11\ sec$. For sit-to-stand movement, COMB is moved from its initial position ${}^0_0\bar{r}_{COMB}\ (t_i) = \{0.3516 \quad 0.6466 \quad 0\}^T\ m$ to the final position ${}^0_0\bar{r}_{COMB}\ (t_f) = \{0.0973 \quad 0.9574 \quad 0\}^T\ m$. The simulations are done for 4s.

**Table 1** Anthropometric properties

| Links | | | Moments of inertia with respect to COM and expressed in the body the frame (kg·m$^2$) | | | Products of inertia with respect to COM and expressed in the body frame (kg·m$^2$) | | |
|---|---|---|---|---|---|---|---|---|
| | | | $I_{xx}$ | $I_{yy}$ | $I_{zz}$ | $I_{xy}=I_{yx}$ | $I_{xz}=I_{zx}$ | $I_{yz}=I_{zy}$ |
| | **Mass (kg)** | **Length (m)** | | | | | | |
| HAT | 46.17 | 0.83 | 0.64 | 2.58 | 2.25 | -0.03 | $3.8\times10^{-4}$ | 0.002 |
| Hip | 8.92 | 0.385 | 0.02 | 0.11 | 0.11 | 0.006 | 0.006 | $5.29\times10^{-4}$ |
| Knee | 3.48 | 0.44 | 0.0067 | 0.05 | 0.05 | -0.001 | -0.001 | $2.6\times10^{-4}$ |
| Ankle | 0.87 | 0.11 | $5.2\times10^{-4}$ | 0.002 | 0.002 | $1.9\times10^{-4}$ | $-1.3\times10^{-4}$ | $3.1x10^{-5}$ |

The parameters of different couplings and the constant multipliers are chosen after performing several progressive simulations and analysis. This is analogous to the progressive learning process which the CNS would have performed for Sit-to-stand motion.

**Table 2** Properties of Muscular Links

| Elements names | Values |
|---|---|
| $C_s$ | $1.01 \times 10^{-5}$ F |
| $C_p$ | $3.125 \times 10^{-4}$ F |
| B | 1200 $\Omega$ |
| m | 1 g |
| $m_1$ | 70 g |
| $B_{gto}$ | 3200 $\Omega$ |
| $C_{gto}$ | 0.001 F |
| $R_{sp}$ | 1200 $\Omega$ |
| $C_{sp}$ | 0.001 F |
| $C_{sr}$ | $2.5 \times 10^{-4}$ F |
| $m_2$ | 1200 g |

The viscoelastic properties of translational couplings and ground are given in Table 2. The properties of model-A and that of model-V are similar to each other. These parameters are selected such that when the joint is subjected to nominal loading conditions then the relative translational movement of two points of the adjacent links joined by a translational coupling may be permitted to move.

For the ankle joint, the translational stiffness in each direction is $10^8$ N/m, which implies that the application of a force due to the weight of a mass of 100 kg produces a deformation of approximately 0.01 mm. Similarly, the implication of the stiffness values for knee and hip joints and the ground translational coupling can be explained. Damping is chosen to dampen out the oscillations.

Table 4 shows the rotational stiffness and damping values that were explored in order to relieve the limitations on rotational motion about the $x_0$ and $y_0$ directions. The

rotational stiffness of $10^5$ Nm/rad in both directions suggests that a torque owing to the weight of a mass of 100 kg placed at 1 m from the axis of rotation will create a deformation of roughly 0.01 rad. The constant multipliers of the nonlinear C and R elements for CRC's are shown in the last column. The constant multiplier of the nonlinear C element is set to 5 Nm, such that opposing torque does not exceed 10 Nm at 80% of the maximum permitted deformation of the cushion at the joint limits.

**Table 3** Viscoelastic properties of translational couplings (TC) and ground couplings

| Couplings | X-direction | | Y-direction | | Z-direction | |
|---|---|---|---|---|---|---|
| | Translational Stiffness (N/m) and damping (N.s/m) | | Translational Stiffness (N/m) and damping (N.s/m) | | Translational Stiffness (N/m) and damping (N.s/m) | |
| TC1 | C=$10^8$ | R=$10^4$ | C=$10^8$ | R=$10^4$ | C=$10^8$ | R=$10^4$ |
| TC2 | C=$5 \times 10^7$ | R=$9 \times 10^3$ | C=$5 \times 10^7$ | R=$9 \times 10^3$ | C=$5 \times 10^7$ | R=$9 \times 10^3$ |
| TC3 | C=$4 \times 10^7$ | R=$8 \times 10^3$ | C=$4 \times 10^7$ | R=$8 \times 10^3$ | C=$4 \times 10^7$ | R=$8 \times 10^3$ |
| Ground | C=$6 \times 10^8$ | R=$10^4$ | C=$6 \times 10^8$ | R=$10^4$ | C=$6 \times 10^8$ | R=$10^4$ |

The maximum and minimum limits of rotation for Hip, Knee and Ankle joints in terms of joint angles along with the maximum permitted deformation on either side of the limits are tabulated in Table 5. These limits for model-V include physiological constraints as well as motion-related constraints. These limits are substituted form Soni & Vaz (2021). Furthermore, only physiological constraints were considered for the model-A, and the limitations were set in accordance with Roaas and Andersson (1982).

**Table 4** Viscoelastic properties of CRC's

| Coupling | X-direction | | Y-direction | | Z-direction | |
|---|---|---|---|---|---|---|
| | Rotation stiffness & damping (Nm/rad) | | Rotation stiffness & damping (Nm/rad) | | Constant multipliers C and R (Nm/rad) | |
| CRC | C= $10^5$ | R=$10^2$ | C= $10^5$ | R=$10^2$ | C=5 | R=20 |

The maximum allowable deformation on either side of the limits is determined so that the limits initially serve as soft cushions and gradually become rigid when the deformation on either side of the limits approaches the maximum permissible deformation. As a result, transients are not stimulated when any of the links reach the rotational limits, resulting in a smooth motion.

Parameters of PID-controllers are tabulated in Table 6. The PD-controller of model-V's proportional gain is set at C=$10^6$ [I]$_{3x3}$ N/m and the derivative gain R=$10^5$ [I]$_{3x3}$ N.s/m. These gains are gathered by hit and error method.

In model-V, the combined effect of damping joints and the CNS learned impedance.is taken into account by the learned damping elements R. The coefficients of R$_3$ in model-V are taken as R$_{ankle}$ = 70 N.m.s/rad, R$_{knee}$ = 3 N.m.s/rad and R$_{hip}$=5 N.m.s/rad for sit-to-stand motion.

**Table 5** Maximum and minimum limits of rotation of joints along with the maximum permissible deformation

| Joints | Joint angle | Model | Max | Min | Max Permissible Deformation |
|--------|-------------|-------|-----|-----|------------------------------|
| Ankle | $_{Ankle\_V}^{Knee\_V}\theta_{Knee\_Vz}$ | | 90° | 78° | 6° |
| Knee | $_{Knee\_V}^{Hip\_V}\theta_{Hip\_Vz}$ | Model-V | 0° | -100° | 4° |
| Hip | $_{Hip\_V}^{HAT\_V}\theta_{HAT\_Vz}$ | | 117° | 0° | 8° |
| Ankle | $_{Ankle\_A}^{Knee\_A}\theta_{Knee\_Az}$ | | 106° | 50° | 6° |
| Knee | $_{Knee\_A}^{Hip\_A}\theta_{Hip\_Az}$ | Model-A | 0° | -143° | 4° |
| Hip | $_{Hip\_A}^{HAT\_A}\theta_{HAT\_Az}$ | | 130° | -10° | 8° |

It is assumed that the CNS learns these values in order to efficiently carry out Sit-to-stand motions. These parameters are adjusted for simulation by tracking the intermediate poses in a series of progressive simulations for the Sit-to-stand motions.

**Table 6** Parameters of PID controllers

| Joints | Proportional gain (N.m/rad) | Derivative gain (N.m.s/rad) | Integral gain (N.m/rad) |
|--------|------------------------------|------------------------------|--------------------------|
| PID$_{ankle}$ | C=5x$10^4$ | R=5x$10^3$ | Se=5x$10^3$ |
| PID$_{knee}$ | C=4x$10^4$ | R=4x$10^3$ | Se=4x$10^3$ |
| PID$_{hip}$ | C=3x$10^4$ | R=3x$10^3$ | Se=3x$10^3$ |

In order to guarantee that the hip and knee joints move more freely than the ankle joint at the start of the Sit-to-stand motions, the ankle joint must have larger coefficients.

This is similar to the natural Sit-to-stand motions, in which the hip and knee joints move rather freely, but the ankle joint seems restricted. Furthermore, the physiological damping elements in model-A solely consider the impact of joint damping. The coefficients of the physiological damping elements in the model-A are taken according to the literature Mizrahi et al. (1988), McFaull & Lamontagne (1998) and Tafazzoli & Lamontagne (1996).

For sit-to-stand motion, these values are $R_{ankle} = 2$ N.m.s/rad, $R_{knee} = 1.5$ N.m.s/rad and $R_{hip}=3$ N.m.s/rad.

## 6.2 Simulations results and discussion

Trajectories of COMB have been reported in earlier studies for sit-to-stand motion by Hughes et al. (1994), Kralj et al. (1990) and Li et al (2021). COM-V tracks the desired trajectory COMB for both Sit-to-stand motions. Furthermore, the COM-A follows the desired course by tracking the trajectory of COM-V.
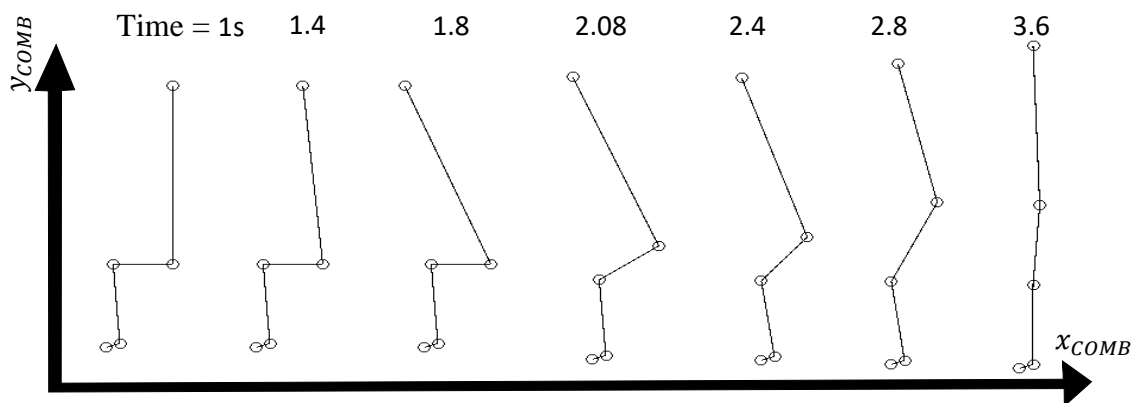


**Figure 15** Intermediate postures of model-A during sit-to-stand motion

Figure 15 shows the intermediate postures of motion produced from the simulation of the model-A for Sit-to-stand motion correspondingly. These postures are strikingly similar to the postures of natural Sit-to-stand motion.

Despite the fact that the COMB trajectory is commanded, the model-V automatically selects these intermediate postures. Because, in the model-V, the effort from the PD controller corresponding to the commanded trajectory of COMB is distributed suitably to each link as shown in the bond graph.

Furthermore, simulation results show that the physiological damping, CNS controlled impedances, and limits of rotation of the joints, which were modelled in model-V using learned damping elements and conditional rotational couplings, respectively, play an important role in achieving natural postures during Sit-to-stand motions.



(a)                                                    (b)
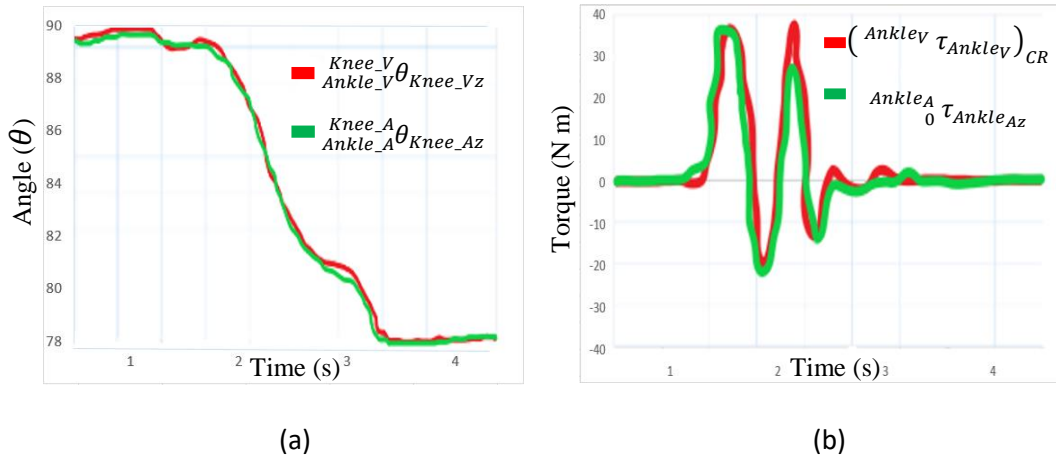
**Figure 16** Ankle joint. a) Joint angle. b) Joint torque

Figure 16 shows the joint angles and torque for ankle joint. For sit-to-stand motion, the approximate tracking errors between joint angles obtained from model-V are $1°$, $3°$ and $4°$ for ankle, knee and hip joints, respectively. It can be observed that joint angle trajectories of model-A closely follow the joint angle trajectories of model-V. Similar results of joint angle trajectories have been obtained in Soni & Vaz (2021).



(a)                                                    (b)

**Figure 17** Knee joint. a) Joint angle. b) Joint torque

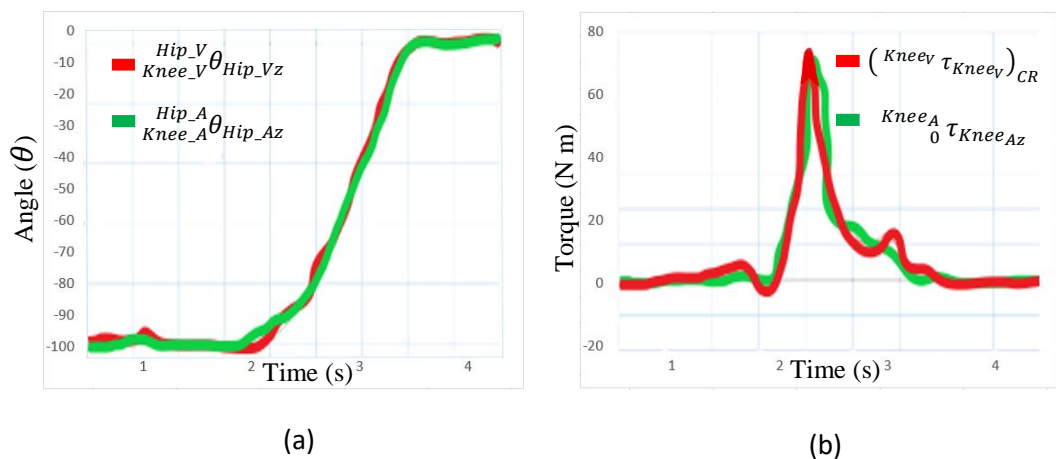It can be observed from Figure 17, that the motion of thigh is against gravity at the knee joint. Thus, the joint torque $\left( {}^{Knee_V} \tau_{Knee_V} \right)_{CR}$ acting on the knee joint is slightly higher than the net torque ${}^{Knee_A}_{0} \tau_{Knee_{Az}}$. The physiological damping at the knee joint will resist the motion when the motion is against gravity. Therefore, the PID-controller of the knee joint has to overcome that resistance which results in more torque to be produced than the net torque acting on the respective joint.

In human body, the muscles produce torque or power and the function of muscles is performed by PID-controller in the model-A. When joint torque at ankle is positive, it is called dorsiflexion torque and when it is negative, it is called plantar flexion torque. For knee joint, when torque is positive, it is called as extension torque and when torque is negative, it is called as flexion torque. When torque is positive at hip joint, it is referred to as flexion torque and when it is negative, it is referred to as extension torque.



(a)  (b)
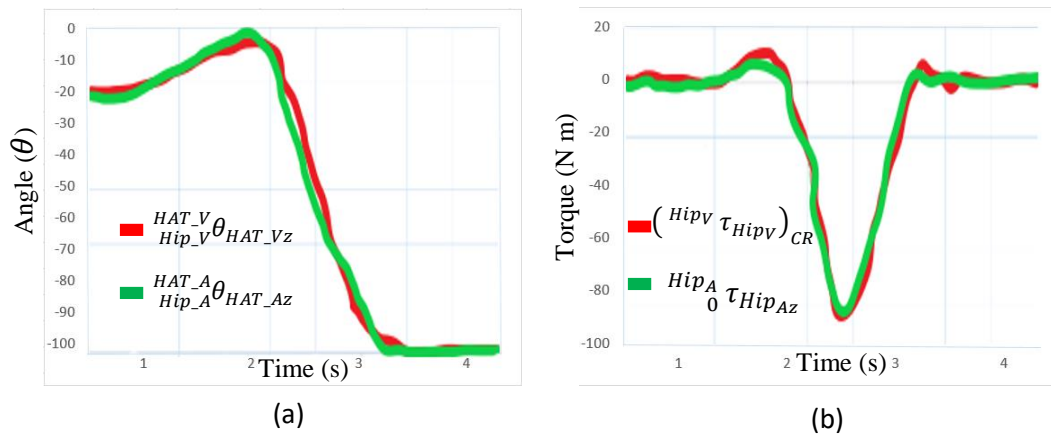
**Figure 18** Hip joint. a) Joint angle. b) Joint torque

## 6.3 Comparative analysis

For ankle joint, dorsiflexion torque of 38 N.m acts at approximately 1.53s. The maximum plantar flexion torque of -22 N.m acts at 1.8s. Ankle joint torque becomes nearly zero at 3.3s approximately. The posture of actual system at the end of sit-to-stand motion is approximately upright due to which the torque requirement at each joint towards the end of the motion should be very less as the COMB lies within the base of the support.

The maximum knee joint torque of 75 N.m is observed at approximately 2.35s. The torque gradually decreases and settles to zero towards the end of the motion as the extension of the knee joint torque progresses.

For hip joint, the maximum flexion torque of 17 N.m is observed at 1.8s at the start of the forward motion of the HAT. At the start of the extension of hip joint, a maximum extension torque of -91 N.m is observed at 2.5s approximately. Almost similar profiles of the knee and hip joint torques have been observed in studies conducted by Soni & Vaz (2021, Mak et al. (2003) and Roebroeck et al. (1994).

The model used is non-linear but due to the essentiality of the parameters chosen and fine tuning of PID controllers, we get high gains therefore we obtain results that are closer to those of a linear model.

When comparing joint torque dynamics with those presented in Sultan et al. (2021) notable observational differences are found as given in Table 7. In this case, while this study has the lower ankle, knee, and hip torque values, Sultan et al. have the highest torque values. For example, in the ankle case, while the dorsiflexion torque in your study is 38 N.m., it is 1250 N.m. for Sultan et al. (2021). The plantar flexion in this study has -22 Nm N.m. and -950 N.m. for the referenced study case. Similarly, for the knee and hip cases, this study shows lower maximum torque than the results obtained in Sultan et al. (2021).

**Table 7** Comparison of joint torque profiles between research studies

| Joint | Parameters | Torque profiles obtained | Torque profiles (Sultan et al. 2021) |
|-------|-----------|--------------------------|--------------------------------------|
| Ankle | Dorsiflexion Torque (N.m) | 38 N.m at 1.53s | 1250 N.m |
| | Plantar Flexion Torque (N.m) | -22 N.m at 1.8s | -950 N.m |
| Knee | Extension Torque (N.m) | 75 N.m at 2.35s | 1000 N.m |
| | Flexion Torque (N.m) | Gradually settles to 0 | -700 N.m |
| Hip | Flexion Torque (N.m) | 17 N.m at 1.8s | 900 N.m |
| | Extension Torque (N.m) | -91 N.m at 2.5s | -600 N.m |

This study, focusing on dynamic muscle modelling, provides insights into joint torques during sit-to-stand movements. The research by Sultan et al. adopts a stiff model

approach, neglecting muscle dynamics. The consideration of muscle dynamics in the study contributes for the development of a contrast and nuanced torque profile that can be considered to be more physiologically reasonable. However, the higher torque values in Sultan et al. suggest that muscle dynamics play a significant role in the level of joint torques. Therefore, despite significant differences in torque magnitude that was revealed, both of these studies allowed for learning about the biomechanics of the sit-to-stand movements and highlighting the importance of muscle dynamics consideration for the movement analysis and rehabilitation.

# CHAPTER 7

# CONCLUSION

A bond graph model is developed and simulated based on the hypothesis that humans perform sit-to-stand movement by controlling the trajectories of the COMB through CNS and that the muscles play a significant role in improving joint torque during sit-to-stand motion. The developed bond graph consists of two identical systems; one model-A that is the actual system representing the human body and the other model-V representing the virtual system to mimic the behavior of CNS. The model consists of four joints that are Head-arm-trunk, hip, knee and ankle joints.

Anthropometric properties of links representing respective limbs have been considered which are realistic in nature. For the sit-to-stand motion, both physiological constraints and the physiological damping of the joints are considered and modelled in the bond graph. The model utilized in this study takes in account both non-linear stiffness and the damping elements which are used to model the limits of rotation of joints.

The novelty of the developed model is that it considers the contribution of muscles at three joints of the human body during sit-to-stand movement. With the inclusion of physiological constraints, constraints due to nature, physiological damping, impedance and appropriate distribution of effort from the PD controller to each link in the model-V, it automatically determines the intermediate postures and required joint angle trajectories.

The impedance of joints and limitation of rotation of joints, plays a significant role in achieving the natural postures during sit-to-stand movement. It is assumed that CNS learns these impedances during sit-to-stand motion. The intermediate postures from the simulations results closely resembles the natural postures during sit-to-stand motion.

It is observed that joint angle trajectories, resembles that of the results achieved by Soni & Vaz (2021). The time trajectories of the joint angles and torques are plotted which agree with the earlier studies. The findings based on the simulation results provide adequate confidence in the developed model.

The developed model gives significant insights by inclusion of muscles during the dynamics of sit-to-stand motion. It is observed that lower torque results are achieved and the model is more refined by the inclusion of muscles at the joints. The developed model is generic and would be useful in investigating different control strategies for sit-to-stand and stand-to-sit motions.

The developed model would be helpful for the development of assistance devices such as robotics rehabilitation. For future work, this study can be extended to explore the dynamics of stand-to-sit motions and posture stability.

# REFERENCES

Asker, A., Assal, S. F. M., Ding, M., Takamatsu, J., Ogasawara, T., & Mohamed, A. M. (2017). Modelling of natural sit-to-stand movement based on minimum jerk criterion for natural-like assistance and rehabilitation. Advanced Robotics, 31(17), 901–917. https://doi.org/10.1080/01691864.2017.1372214

Aylar, M. F., Dionisio, V. C., & Jafarnezhadgero, A. A. (2019). Do the center of mass strategies change with restricted vision during the sit-to-stand task? Clinical Biomechanics, 62, 104–112. https://doi.org/10.1016/j.clinbiomech.2019.01.011

Chen, L., et al. (2020). Bridging the Gap: Integrating Computational Models and Experimental Data for Joint Torque Estimation. Journal of Applied Biomechanics, 36(2), 210–225.

Crowninshield, R. D., & Brand, R. A. (1981). A physiologically based criterion of muscle force prediction in locomotion. Journal of biomechanics, 14(11), 793-801.

Denizdurduran, B., Markram, H., & Gewaltig, M.O. (2022). Optimum trajectory learning in musculoskeletal systems with model predictive control and deep reinforcement learning. Biol Cybern,116,711–726.https://doi.org/10.1007/s00422-022-00940-x

Dumas, R., & Wojtusch, J. (2017). Estimation of the Body Segment Inertial Parameters for the Rigid Body Biomechanical Models Used in Motion Analysis. In Handbook of Human Motion. Springer International Publishing. https://doi.org/10.1007/978-3-319-30808-1

F. Kitayama, R. Kondo and R. Endo, "Improvement of Transmission Torque Characteristics of Strain Wave Gear with Magnets," 2023 IEEE International Magnetic Conference - Short Papers (INTERMAG Short Papers), Sendai, Japan, 2023, pp. 1-2, doi: 10.1109/INTERMAGShortPapers58606.2023.10228713.

Houk, J. C. (1988). Regulation of muscle contraction: neural control. In Exercise: Regulation and integration of multiple systems (pp. 403-439). Elsevier.

Iqbal, K. (2021). Model Predictive Control of Biomechanical Sit-to-Stand. IFAC-PapersOnLine, 54(20), 96–101. https://doi.org/10.1016/j.ifacol.2021.11.159

Johnson, M. R., et al. (2021). Understanding Joint Torque: A Multidisciplinary Perspective. Biomechanics Journal, 25(3), 112–129.

Laschowski, B., Razavian, R. S., & McPhee, J. (2021). Simulation of Stand-to-Sit Biomechanics for Robotic Exoskeletons and Prostheses With Energy Regeneration. IEEE Transactions on Medical Robotics and Bionics, 3(2), 455–462. https://doi.org/10.1109/TMRB.2021.3058323

Li, J., Xue, Q., Yang, S., Han, X., Zhang, S., Li, M., & Guo, J. (2021). Kinematic analysis of the human body during sit-to-stand in healthy young adults. Medicine, 100(22), e26208. https://doi.org/10.1097/MD.0000000000026208

Liang, S., Zhao, G., Zhang, Y., Diao, Y., & Li, G. (2021). Stability region derived by center of mass for older adults during trivial movements. Biomedical Signal Processing and Control, 69, 102952. https://doi.org/10.1016/j.bspc.2021.102952

Lockhart, T. E., & Woldstad, J. C. (2003). Effects of age-related gait changes on biomechanics, energetics, and gait stability. Gait & posture, 17(2), 204-214.

M. Mughal and K. Iqbal, "H∞ controller synthesis for a physiological motor control system modeled with bond graphs," 2006 IEEE Conference on Computer Aided Control System Design, 2006 IEEE International Conference on Control Applications, 2006 IEEE International Symposium on Intelligent Control, 2006, pp. 947-952, doi: 10.1109/CACSD-CCA-ISIC.2006.4776772.

McFaull, S. R., & Lamontagne, M. (1998). In vivo measurement of the passive viscoelastic properties of the human knee joint. Human Movement Science, 17(2), 139–165. https://doi.org/10.1016/S0167-9457(97)00027-4

Migalev, A.S., Vigasina, K.D., & Gotovtsev, P.M. (2022). A review of motor neural system robotic modeling approaches and instruments. Biol Cybern, 116, 271–306. https://doi.org/10.1007/s00422-021-00918-1

Mizrahi, J., Ramot, Y., & Susak, Z. (1988). Damping and elastic response of the human ankle to in vivo sudden eversion motion. Proceedings of the Annual International Conference of the IEEE Engineering in Medicine and Biology Society, 2, 629–630 vol.2. https://doi.org/10.1109/IEMBS.1988.94803

Mughal, Asif Mahmood, & Iqbal, K. (2012). Physiological LQR Design for Postural Control Coordination of Sit-to-Stand Movement. Cognitive Computation, 4(4), 549–562. https://doi.org/10.1007/s12559-012-9160-5

Mughal, Asif M., and Kamran Iqbal. "Bond graph modelling and optimal controller design for physiological motor control system." *International Journal of Modelling and Simulation* 33.2 (2013): 93-101.

Rafique, S., Najam-ul-Islam, M., Shafique, M., & Mahmood, A. (2020). Neuro-fuzzy control of sit-to-stand motion using head position tracking. *Measurement and Control*, 53(7-8), 1342-1353. https://doi.org/10.1177/0020294020938079

Sultan, N., Najam ul Islam, M., & Mahmood Mughal, A. (2020). Nonlinear robust compensator design for postural control of a biomechanical model with delayed feedback. *Measurement and Control*, 53(3–4), 679–690. https://doi.org/10.1177/0020294019900285

Sultan, N., Islam, M. N. U., Mughal, A. M., & Iqbal, K. (2021). High-gain observer-based nonlinear control scheme for biomechanical sit to stand movement in the presence of sensory feedback delays. PLOS ONE, 16(8), e0256049. https://doi.org/10.1371/journal.pone.0256049

Nadia Sultan, Muhammad Najam ul Islam, and Asif Mahmood Mughal. (2021). Nonlinear postural control paradigm for larger perturbations in the presence of neural delays. Biol. Cybern. 115, 4 (Aug 2021), 397–414. https://doi.org/10.1007/s00422-021-00889-3.

Smith, J. A., et al. (2022). Advancements in Bond Graph Modelling for Simulating Muscle-Driven Joint Movements. Journal of Biomechanical Engineering.

Soni, V., & Vaz, A. (2021). A Bond Graph Model for the Estimation of Torque Requirements at the Knee Joint During Sit-to-Stand and Stand-to-Sit Motions. Lecture Notes in Mechanical Engineering. DOI: 10.1007/978-981-16-0550-5_154

Sultan N, Mughal AM, Islam MNu, Malik FM (2021) High-gain observer-based nonlinear control scheme for biomechanical sit to stand movement in the presence of sensory feedback delays. PLoS ONE 16(8): e0256049. https://doi.org/10.1371/journal.pone.0256049

Tafazzoli, F., & Lamontagne, M. (1996). Mechanical behaviour of hamstring muscles in low-back pain patients and control subjects. Clinical Biomechanics, 11(1), 16–24.

Tan, Q. (2020). Lower extremity assisted exoskeleton for people who need rehabilitation training and stairs assistance. Journal of Physics: Conference Series, 1650(2), 022036. https://doi.org/10.1088/1742-6596/1650/2/022036

Taniai, Y., Naniwa, T., & Nishii, J. (2022). Optimal reaching trajectories based on feedforward control. Biol Cybern, 116, 517–526. https://doi.org/10.1007/s00422-022-00939-4

Wakeling, James M., Míriam Febrer-Nafría, and Friedl De Groote. "A review of the efforts to develop muscle and musculoskeletal models for biomechanics in the last 50 years." Journal of Biomechanics (2023): 111657.

Walter, J.R., Günther, M., Haeufle, D.F.B., et al. (2021). A geometry- and muscle-based control architecture for synthesizing biological movement. Biol Cybern, 115, 7–37. https://doi.org/10.1007/s00422-020-00856-4

Zajac, F. E. (1989). Muscle and Tendon: Properties, Models, Scaling, and Application to Biomechanics and Motor Control. Critical Reviews in Biomedical Engineering, 17(4), 359–411.

Zoheb, Madiha, and A. M. Mughal. "Bond Graph Modelling and PID Controller Stabilization of Single link Mechanical Model." International Conference on Modelling and Simulation. 2013.

## APPENDIX A

## TURNITIN ORIGINALITY REPORT

**ORIGINALITY REPORT**

| **13%** SIMILARITY INDEX | **9%** INTERNET SOURCES | **8%** PUBLICATIONS | **4%** STUDENT PAPERS |
| --- | --- | --- | --- |

**PRIMARY SOURCES**

| | | |
| --- | --- | --- |
| 1 | prr.hec.gov.pk<br>Internet Source | 2% |
| 2 | Submitted to Higher Education Commission Pakistan<br>Student Paper | 1% |
| 3 | mafiadoc.com<br>Internet Source | 1% |
| 4 | www.researchgate.net<br>Internet Source | 1% |
| 5 | Rochdi Merzouki, Arun Kumar Samantaray, Pushparaj Mani Pathak, Belkacem Ould Bouamama. "Intelligent Mechatronic Systems", Springer Nature, 2013<br>Publication | 1% |
| 6 | biomedical-engineering-online.biomedcentral.com<br>Internet Source | <1% |
| 7 | Ju Biao Yao, Zhu Ming Cao, Jia Tian Guo. "The Research of Hybrid Bond Graph Modeling", Journal of Physics: Conference Series, 2018<br>Publication | <1% |

| 8 | Wolfgang Borutzky. "Bond Graph Methodology", Springer Science and Business Media LLC, 2010<br>Publication | <1% |
|---|---|---|
| 9 | hdl.handle.net<br>Internet Source | <1% |
| 10 | "Handbook of Human Motion", Springer Science and Business Media LLC, 2018<br>Publication | <1% |
| 11 | "Machines, Mechanism and Robotics", Springer Science and Business Media LLC, 2022<br>Publication | <1% |
| 12 | Asif Mahmood Mughal. "Real Time Modeling, Simulation and Control of Dynamical Systems", 'Springer Science and Business Media LLC', 2016<br>Internet Source | <1% |
| 13 | es.scribd.com<br>Internet Source | <1% |
| 14 | Submitted to University of Warwick<br>Student Paper | <1% |
| 15 | ebin.pub<br>Internet Source | <1% |
| 16 | repositorio.uta.edu.ec<br>Internet Source | <1% |

17 "Climbing and Walking Robots", Springer Science and Business Media LLC, 2006
Publication
<1%

18 Samantaray, A.K.. "Diagnostic bond graphs for online fault detection and isolation", Simulation Modelling Practice and Theory, 200604
Publication
<1%

19 C. Izaguirre-Espinosa, A. Muñoz-Vazquez, A. Sánchez-Orta, V. Parra-Vega, R. Garcia-Rodriguez, P. Castillo, D. Arreguín-Jasso. "Stabilization of Tangent and Normal Contact Forces for a Quadrotor subject to Disturbances", 2022 IEEE/RSJ International Conference on Intelligent Robots and Systems (IROS), 2022
Publication
<1%

20 patents.google.com
Internet Source
<1%

21 bartlab.org
Internet Source
<1%

22 Advances in Computational Multibody Systems, 2005.
Publication
<1%

23 Zhao, Yu. "Intelligent Control and Planning for Industrial Robots.", University of California, Berkeley, 2019
<1%

Publication

24   F. Kitayama, R. Kondo, R. Endo. "Improvement of Transmission Torque Characteristics of Strain Wave Gear with Magnets", 2023 IEEE International Magnetic Conference - Short Papers (INTERMAG Short Papers), 2023
Publication

<1%

25   Saumitra Barman, Manoranjan Sinha. "Satellite Attitude Control Using Double-Gimbal Variable-Speed Control Moment Gyroscope: Single-Loop Control Formulation", Journal of Guidance, Control, and Dynamics, 2023
Publication

<1%

26   dokumen.pub
Internet Source

<1%

27   research.library.mun.ca
Internet Source

<1%

28   Kai Sasaki, Minatsu Sugimoto, Taisei Sugiyama, Diego Felipe Paez Granados, Kenji Suzuki. "Child-Sized Passive Exoskeleton for Supporting Voluntary Sitting and Standing Motions", 2018 IEEE/RSJ International Conference on Intelligent Robots and Systems (IROS), 2018
Publication

<1%

29 **Submitted to University of Melbourne**
Student Paper

<1%

30 Clark R. Dickerson, Don B. Chaffin, Richard E.
Hughes. "A mathematical musculoskeletal
shoulder model for proactive ergonomic
analysis", Computer Methods in
Biomechanics and Biomedical Engineering,
2007
Publication

<1%

31 vts.uni-ulm.de
Internet Source

<1%

32 Borutzky. "Multibody Systems", Bond Graph
Methodology, 2010
Publication

<1%

33 Dean C. Karnopp, Donald L. Margolis, Ronald
C. Rosenberg. "System Dynamics", Wiley,
2012
Publication

<1%

34 El Feki, M., A. Jardin, W. Marquis-Favre, L.
Krahenbuhl, and D. Thomasset. "Structural
analysis by bond graph approach: duality
between causal and bicausal procedures",
Proceedings of the Institution of Mechanical
Engineers Part I Journal of Systems and
Control Engineering, 2012.
Publication

<1%

35 J.A. Gonzalez, C. Sueur. "Unknown Input Observer with stability: A Structural Analysis Approach in Bond Graph", European Journal of Control, 2018
Publication
<1%

36 Kenshi Saho, Kouki Sugano, Kazuki Uemura, Michito Matsumoto. "Screening of apathetic elderly adults using kinematic information in gait and sit-to-stand/stand-to-sit movements measured with Doppler radar", Health Informatics Journal, 2021
Publication
<1%

37 Mechatronics by Bond Graphs, 2003.
Publication
<1%

38 Rodolfo Borges Parreira, Jamile Benite Palma Lopes, Lorraine Barbosa Cordeiro, Manuela Galli, Claudia Santos Oliveira. "Assessment of functional mobility and gait during a timed up and go test in adults with total blindness", Journal of Bodywork and Movement Therapies, 2023
Publication
<1%

39 discovery.researcher.life
Internet Source
<1%

40 fenix.tecnico.ulisboa.pt
Internet Source
<1%

orca.cardiff.ac.uk

**41** Internet Source

<1%

**42** projekter.aau.dk
Internet Source

<1%

**43** LEE, JONG-WON, HYOGON KIM, JAEHO JANG, and SANGDEOK PARK. "STUDY ON THE CONTROL BASED ON VIRTUAL SPRING MODEL FOR LOWER EXTREMITY EXOSKELETON", Adaptive Mobile Robotics, 2012.
Publication

<1%

**44** Raphael Pfaff, Keith J. Burnham. "On Abstraction and Interpretability: A Behavioural Perspective", 2008 19th International Conference on Systems Engineering, 2008
Publication

<1%

**45** Sadiq J. Hamandi, Duaa M. Ruken. "Biomechanical study with kinematic and kinetic descriptions of the effect of high-heeled shoes in healthy adult females based on gait analysis", IOP Conference Series: Materials Science and Engineering, 2020
Publication

<1%

**46** citeseerx.ist.psu.edu
Internet Source

<1%

journals.lww.com

47  Internet Source                                                <1%

48  pure.roehampton.ac.uk
    Internet Source                                                <1%

49  spiral.imperial.ac.uk
    Internet Source                                                <1%

50  "Bond Graphs for Modelling, Control and                        <1%
    Fault Diagnosis of Engineering Systems",
    Springer Science and Business Media LLC,
    2017
    Publication

51  AliAsghar MohammadiNasrabadi, John                            <1%
    McPhee. "Preliminary optimization of cup-
    implant orientation in total-hip arthroplasty
    using a parametric predictive analysis of
    lower-limb dynamics influenced by spine
    stiffness", Multibody System Dynamics, 2023
    Publication

52  Amankwah, K.. "A model-based study of                         <1%
    passive joint properties on muscle effort
    during static stance", Journal of
    Biomechanics, 2006
    Publication

53  Anil Kumar Narwal, Anand Vaz, K.D. Gupta.                     <1%
    "Study of dynamics of soft contact rolling
    using multibond graph approach",
    Mechanism and Machine Theory, 2014

Publication

54 Asif M. Mughal, Kamran Iqbal. "MODELLING AND ANALYSIS PHYSIOLOGICAL MOTOR CONTROL USING BOND GRAPH", IFAC Proceedings Volumes, 2006
Publication

<1%

55 B. Ould-Bouamama, R. El Harabi, M.N. Abdelkrim, M.K. Ben Gayed. "Bond graphs for the diagnosis of chemical processes", Computers & Chemical Engineering, 2012
Publication

<1%

56 Mohammad Hassan Nematollahi, Seyyed Arash Haghpanah, Sajjad Taghvaei. "Inverse dynamic tracking control of sitting and standing movement", 2018 25th National and 3rd International Iranian Conference on Biomedical Engineering (ICBME), 2018
Publication

<1%

57 Rakshit, Sourav, and Srinivas Akella. "A trajectory optimization formulation for assistive robotic devices", 2016 IEEE International Conference on Robotics and Automation (ICRA), 2016.
Publication

<1%

58 Rod Barrett, A.J. 'Knoek' van Soest, Rob Neal. "A computer-graphics model of muscle activation and contraction dynamics", Sports Biomechanics, 2002

<1%

Publication

59 Ruey-Chyi Wu. "Development of an Intelligent Virtualization Platform Key Metrics Monitoring System: Collaborative Implementation with Self-Training and Bagging Algorithm", Research Square Platform LLC, 2024
Publication
<1%

60 Smith, Lorcan Stuart Peter Stillwell. "Bond Graph Modelling of Physical Systems.", University of Glasgow (United Kingdom), 2003
Publication
<1%

61 Taku Komura. "A Muscle-based Feed-forward Controller of the Human Body", Computer Graphics Forum, 9/1997
Publication
<1%

62 Thatte, Nitish. "Design and Evaluation of Robust Control Methods for Robotic Transfemoral Prostheses.", Carnegie Mellon University, 2020
Publication
<1%

63 bahria.edu.pk
Internet Source
<1%

64 idoc.pub
Internet Source
<1%

65 open.library.ubc.ca
Internet Source
<1%

66 pubmed.ncbi.nlm.nih.gov
Internet Source
<1%

67 ruor.uottawa.ca
Internet Source
<1%

68 salford-repository.worktribe.com
Internet Source
<1%

69 Ashraf A. Zeid, James L. Overholt. "Singularly perturbed formulation: Explicit modeling of multibody systems", Journal of the Franklin Institute, 1995
Publication
<1%

70 Danforth, Shannon M.. "Human Prediction and Robotic Lower-Limb Prosthesis Planning for Safe Perturbation Recovery during Motion", University of Michigan, 2022
Publication
<1%

71 Davis, John Jerome, IV. "Understanding Internal Biomechanical Loads During Running Using Wearable Sensors", Indiana University, 2023
Publication
<1%

72 de Abreu, Jéssica. "Reinforcement Learning Control of Upper-Limb Models Actuated by Chronically Paralyzed Muscles", Case Western Reserve University, 2023
Publication
<1%

73 | "Bond Graph Modelling of Engineering Systems", Springer Science and Business Media LLC, 2011
Publication | <1%

74 | Armin Hakkak Moghadam Torbati, Shahab Jami, Hamid Reza Kobravi. "Is the Hénon map able to predict the interaction dynamics between the knee and hip joints emerged during sit-to-stand movement?", Biomedical Physics & Engineering Express, 2022
Publication | <1%

75 | Bera, T. K., R. Merzouki, B. Ould Bouamama, and A. K. Samantaray. "Force control in a parallel manipulator through virtual foundations", Proceedings of the Institution of Mechanical Engineers Part I Journal of Systems and Control Engineering, 2012.
Publication | <1%

76 | Buyun Wang, Yi Liang, Dezhang Xu, Zhihong Wang, Jing Ji. "Design on electrohydraulic servo driving system with walking assisting control for lower limb exoskeleton robot", International Journal of Advanced Robotic Systems, 2021
Publication | <1%

Exclude quotes          On
Exclude bibliography    On

Exclude matches         Off